# Integrability in anyonic quantum spin chains via a composite height model

Paata Kakashvili[*] and Eddy Ardonne

*Nordita, Roslagstullsbacken 23, SE-106 91 Stockholm, Sweden*
(Received 10 October 2011; published 15 March 2012)

Recently, properties of collective states of interacting non-Abelian anyons have attracted considerable attention. We study an extension of the "golden chain model," where two- and three-body interactions are competing. Upon fine tuning the interaction, the model is integrable. This provides an additional integrable point of the model, on top of the integrable point, when the three-body interaction is absent. To solve the model, we construct a new, integrable height model, in the spirit of the restricted solid-on-solid model solved by Andrews *et al*. [J. Stat. Phys. **35**, 193 (1984)]. The heights in our model live on both the sites and links of the square lattice. The model is solved by means of the corner transfer matrix method. We find a connection between local height probabilities and characters of a conformal field theory governing the critical properties at the integrable point. In the antiferromagnetic regime, the criticality is described by the $Z_k$ parafermion conformal field theory, while the $\frac{\mathrm{su}(2)_1 \times \mathrm{su}(2)_1 \times \mathrm{su}(2)_{k-2}}{\mathrm{su}(2)_k}$ coset conformal field theory describes the ferromagnetic regime.

## I. INTRODUCTION

The last half decade has seen a big increase in the interest of topological phases of matter. In this paper, we study a model which is inspired by the prototype of a topological phase, namely the (fractional) quantum Hall effect. It has been conjectured that there exist fractional quantum Hall states with excitations which exhibit non-Abelian statistics.[1] One of the key properties of this type of excitation, called non-Abelian anyons, is that a topological state with a number of non-Abelian anyons present is degenerate. The number of degenerate states is exponential, while the energy splitting in real systems decays exponentially with the average distance between the non-Abelian anyons.

An important question which arises concerns what happens if the anyons are close to one another, such that they start interacting. To this end, a one-dimensional (1D) model of interacting anyons was constructed in Ref. 2, called the "golden chain," because it was based on Fibonacci anyons. The philosophy behind this model was to stay as closely as possible to a Heisenberg model of interacting spins. In fact, the golden chain is precisely that, a Heisenberg model with two-body nearest-neighbor interactions, but for anyons instead of spins. The phase diagram of such anyonic Heisenberg models turns out to be rich, even richer than the phase diagrams of the ordinary spin case. We do not embark on a long discussion of the phase diagrams of these models here, but focus in the next section on one particular example of interest for the current paper, an extension of the golden chain model with competing two- and three-body interactions.[3] We would like to point out that studying the effects of interacting anyons in 1D gives insight into the fate of interacting anyons in two-dimensional (2D) systems. The interactions between the anyons can nucleate a new topological liquid, and the collective behavior of the 1D chain describes the boundary between the original and nucleated topological phases (see Refs. 4–7 for related work).

An interesting property of the anyonic chain models is that they exhibit (fine-tuned) points, at which it is possible to solve the model exactly. Obviously, having access to an exact solution, even though such a solution is only available at special points, greatly enhances the understanding of the model. The golden chain (with a two-body interaction) and its cousins, which are obtained by replacing the Fibonacci anyons by anyons based on su(2)$_k$, can be mapped onto a 2D classical statistical mechanics model, namely the restricted solid-on-solid (RSOS) model, introduced and solved by Andrews, Baxter, and Forrester (ABF).[8] This RSOS model consists of heights living on the sites of the square lattice. Plaquettes are weighted depending on the heights of the sites forming the plaquettes. To solve the model, ABF employed the so-called corner transfer matrix (CTM) method.[9] It was found that the model exhibits various ordered phases, separated by critical points. The connection between the critical exponents and conformal field theory (CFT) was made by Huse.[10] The anyonic chains correspond to the RSOS model at the critical point and are therefore critical themselves and governed by the same CFT.[2]

The CTM method allows one to calculate, in the limit of infinite lattice size, the probability for a site in the bulk to have a particular height. Interestingly, it has been observed that off-critical local height probabilities of integrable models are intimately related to partition functions of the associated critical theories in a finite box with appropriate boundary conditions.[11] Moreover, close to critical points, these height probabilities are given in terms of characters of a CFT, which describes the critical behavior of the model.[12] The characters stemming from the height probabilities in the RSOS model are, for instance, given in Ref. 13. These characters can be interpreted in terms of fractional exclusion statistics[14] or, more specifically, a non-Abelian version thereof.[15,16] In light of the current paper, we would like to point out that the height probabilities one obtains for a finite system correspond to finitized characters. Interestingly, the opposite "ends" of these finitized characters correspond to the full characters of two different conformal field theories, in the large size limit. These two different conformal field theories describe the critical properties of different critical points of the (RSOS) model. In terms of the anyonic chains, these two critical points are related to each other by changing the overall sign of the interaction.

In this paper, we examine an integrable point of anyonic chains with competing two- and three-body interaction terms.

To solve the model, we introduce a new statistical mechanics model, which builds on the RSOS model, which has six different types of plaquettes. In our new model, we combine four plaquettes of the RSOS model and shift two of the plaquette weights to obtain a nontrivial generalization. Via this procedure, one obtains a model with 66 different types of plaquettes. This composite height model gives rise to the anyonic chain Hamiltonians of interest via the usual "anisotropic limit." To solve the model, we follow the work of ABF and employ the CTM method to calculate the height probabilities.

A very closely related loop model has been studied in the literature.[17,18] In fact, the $R$ matrix, used to construct the row-to-row transfer matrix, has the same underlying algebraic structure, namely that of the Temperley-Lieb algebra, and the construction of our 2D model is inspired by the work in Refs. 17 and 18. However, the quantum chain of that work is defined on a completely different Hilbert space, in comparison to the anyonic chains. In our case, the Hilbert space does not have a tensor product decomposition, which hinders solving the model by means of the Bethe Ansatz, which is the method used in Refs. 17 and 18 (in their representation, the Hilbert space does have a tensor product decomposition). The Hilbert spaces of the anyonic chains exhibit a nonlocal, topological symmetry, giving rise to a topological quantum number, which can be used to label the eigenstates of Hamiltonians respecting this symmetry (see, for instance, Refs. 2 and 19). In gapped phases where the ground state breaks this symmetry, one finds additional degeneracies. This additional structure, which is intimately tied to the non-Abelian nature of the anyons, seems to be absent in the work of Refs. 17 and 18.

The outline of the paper is as follows. In Sec. II, we briefly introduce the anyonic chain Hamiltonians, starting with the original golden chain, and its generalization by introducing the three-body interaction. We also briefly discuss the anyonic chains based on su(2)$_k$ anyons. In Sec. III, we discuss the connection of the golden chain with the RSOS model. Section IV contains the definition of our composite height model, which builds on the RSOS model. The CTM method is described in Sec. V, which leads to the expressions for the height probabilities. These are used in the Sec. VI to obtain information about the various phases of the model. In Sec. VII, we calculate off-critical local height probabilities in different phases and show that they are given in terms of characters of the CFTs, which govern the corresponding critical points. We conclude in Sec. VIII. In Appendix A, we explicitly give the different types of plaquettes of the composite height model. Appendix B contains various limits of the CTMs, which are used in the main text. Appendix C deals with a certain limit of the plaquettes. Finally, in Appendix D, we give the details of the connection of the various height probabilities with CFT characters.

## II. ANYON CHAINS WITH COMPETING INTERACTIONS

### A. The golden chain

The first model of interacting anyons, introduced in Ref. 2, was dubbed the golden chain. In this model, so-called Fibonacci anyons interact in basically the same way as
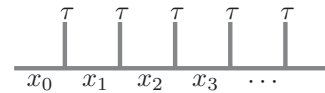


FIG. 1. The fusion chain consisting of Fibonacci anyons. Consistent labelings $(x_0, x_1, \ldots, x_L)$ form the Hilbert space of the anyonic chain.

spins in the Heisenberg spin chain; namely, an energy is assigned depending on the overall spin state of two interacting particles. In the $S = 1/2$ Heisenberg chain the $S = 0$ state of two neighboring spins is favored for antiferromagnetic interactions, while for ferromagnetic interactions the $S = 1$ channel for neighboring spins is favored.

To explain the interaction of the golden chain, we first briefly introduce the notion of (Fibonacci) anyons. A rather extensive introduction to this topic can be found in Ref. 20. The Fibonacci anyon model consists of two types of particles: the "trivial" or vacuum particle **1** and the Fibonacci particle $\tau$. As with ordinary spins, one can combine or fuse these particles and decompose the product. This fusion product is the direct analog of taking tensor products of spins. Contrary to su(2) spin, there is only a finite number of types of particles. In addition, there is no internal quantum number, such as $s_z$. The reason for this will become clear shortly.

The rules for combining the anyons in the Fibonacci model are as follows: $\mathbf{1} \times \mathbf{1} = \mathbf{1}$, $\mathbf{1} \times \tau = \tau$, and $\tau \times \tau = \mathbf{1} + \tau$, the latter being the only nontrivial fusion rule.

Let us take a chain of $L$ $\tau$ anyons. To describe the Hilbert space of this system, it is easiest to think in terms of a so-called fusion chain, as depicted in Fig. 1.

This fusion chain consists of labeled lines, $L$ incoming lines labeled $\tau$, which represent the Fibonacci anyons that form the chain. The lines connecting these incoming $\tau$ anyons are labeled $x_0, x_1$, etc. These labels, which can take the values **1** and $\tau$, are the "degrees of freedom." The set of consistent labelings $(x_0, x_1, \ldots, x_L)$ forms the Hilbert space of the chain. For a labeling to be consistent, the fusion rules have to be satisfied at every vertex. This means that $x_{i+1}$ has to be in the fusion of $x_i \times \tau$. This means that one cannot have $x_i = x_{i+1} = \mathbf{1}$, because this would violate the fusion rule $\mathbf{1} \times \tau = \tau$. Apart from the constraint that no two neighboring labels can both take the value **1**, the labelings are arbitrary. Because of the constraint, the size of the Hilbert space grows as $d^L$, where $d < 2$. It is not so hard to convince oneself that, in fact, $d$ is the golden ratio, $d = \varphi = (1 + \sqrt{5})/2$. In the remainder of the description, we assume periodic boundary conditions, $x_0 = x_L$. In this case, the size of the Hilbert space is given by $\dim \mathcal{H}_L = \mathrm{Fib}(L + 1) + \mathrm{Fib}(L - 1)$, where $\mathrm{Fib}(n)$ is the $n$th Fibonacci number, defined by $\mathrm{Fib}(n) = \mathrm{Fib}(n - 1) + \mathrm{Fib}(n - 2)$ and the initial conditions $\mathrm{Fib}(0) = 0$ and $\mathrm{Fib}(1) = 1$. Loosely speaking, one can say that each Fibonacci anyon has a fractional number of degrees of freedom, namely $d$, explaining the absence of an internal quantum number. More importantly, one cannot assign a local Hilbert space to each anyon. This is the reason we had to resort to the fusion chain to describe the Hilbert space, which cannot be described as a tensor product of local Hilbert spaces, as is the case for ordinary spin chains.

We would like to point out that in the description of the Hilbert space, we did not make use of the braid properties of the Fibonacci anyons. Often the braid properties are used to define the concept of non-Abelian statistics. What we have done here instead is to use the fusion properties of the Fibonacci anyons, which make non-Abelian statistics possible. In particular, in order for non-Abelian statistics to be possible, one needs a Hilbert space whose dimension is at least two. This in turn is possible if one considers particles (anyons) which have multiple fusion channels upon fusion with another particle, such as $\tau \times \tau = \mathbf{1} + \tau$. In the construction of interacting anyonic chains, it is the presence of multiple fusion channels which is the key property of non-Abelian statistics which is utilized. One can consider models in which the explicit, non-Abelian braid properties are used to define the Hamiltonian (see for instance Ref. [20]), but that is not the route we take in the present paper.

We turn our attention to the description of the Hamiltonian. We first concentrate on the Hamiltonian of the original golden chain model. The interaction between two anyons depends on their overall fusion channel. Favoring the overall fusion channel of two neighboring anyons to be $\mathbf{1}$ is called antiferromagnetic, while favoring the $\tau$ channel is called ferromagnetic interaction.

In our description of the Hilbert space in terms of a fusion chain, the fusion channel of two neighboring anyons is not explicit, because the lines associated with these two anyons do not meet in one vertex. One can, however, perform a local basis transformation, which makes this fusion channel explicit. The matrix describing this basis transformation is called the $F$ matrix, which is the direct analog of the $6j$ symbols in the case of su(2) spin. These describe the change of basis between the following two possible ways of describing the Hilbert space of three spins: $(S_1 \otimes S_2) \otimes S_3$ and $S_1 \otimes (S_2 \otimes S_3)$. In Fig. 2, we depict the $F$ matrix in terms of the fusion-chain pictures.

After performing this local basis transformation, the fusion channel of the two neighboring anyons is explicit and is given by $x_i'$. Based on the value of this label (which can be $\mathbf{1}$ or $\tau$), we can now assign the energy by projecting onto the $\mathbf{1}$ or $\tau$ channel. All that is left to do is to perform one more basis transformation to go back to the original basis.

To make the model completely explicit, we have to give the values of the $F$-matrix elements. For the anyon models based on su(2), there exist explicit formulas for the $F$ matrices (see for instance Ref. [21]). We do not go into the details here, but simply give the results for the $F$ symbols we need. Note that there is some degree of freedom in the $F$ symbols; the explicit form we give fixes this. The $F$ symbols we need are specified by specifying the values of $(x_{i-1}, x_i, x_{i+1})$, which can take the values $\{(\mathbf{1}, \tau, \mathbf{1}), (\mathbf{1}, \tau, \tau), (\tau, \tau, \mathbf{1}), (\tau, \mathbf{1}, \tau), (\tau, \tau, \tau)\}$. In addition, we have to specify the degrees of freedom after



FIG. 2. The $F$-matrix elements as a local basis transformation.

the basis transformation $(x_{i-1}, x_i', x_{i+1})$, which can take the values $\{(\mathbf{1}, \mathbf{1}, \mathbf{1}); (\mathbf{1}, \tau, \tau); (\tau, \tau, \mathbf{1}); (\tau, \mathbf{1}, \tau), (\tau, \tau, \tau)\}$. Using this ordering of the states, the $F$ matrix takes the form (highlighting the block structure)

$$F = \begin{pmatrix} 1 & & & & \\ & 1 & & & \\ & & 1 & & \\ & & & d^{-1} & d^{-\frac{1}{2}} \\ & & & d^{-\frac{1}{2}} & -d^{-1} \end{pmatrix}. \quad (1)$$

The inverse transformation is given by the same matrix, because $F = F^{-1}$, as is easily checked by using $d^2 = 1 + d$. We can now easily form the local projection operators $P_{2\text{-body}}^{(\tau)}$ and $P_{2\text{-body}}^{(\mathbf{1})}$, which project onto the $\tau$ and $\mathbf{1}$ channels, that is, give energy to these channels. Hence, $P_{2\text{-body}}^{(\tau)}$ corresponds to the antiferromagnetic interaction. Explicitly, these projection matrices take the form $P_{2\text{-body}}^{(\tau)} = F \cdot \text{diag}(0,1,1,0,1) \cdot F$ and $P_{2\text{-body}}^{(\mathbf{1})} = F \cdot \text{diag}(1,0,0,1,0) \cdot F$. The components of these matrices read $(F_{x_{i+1}}^{x_{i-1},\tau,\tau})_\tau^{\tilde{x}_i} (F_{x_{i+1}}^{x_{i-1},\tau,\tau})_{x_i}^\tau$ and $(F_{x_{i+1}}^{x_{i-1},\tau,\tau})_{\mathbf{1}}^{\tilde{x}_i} (F_{x_{i+1}}^{x_{i-1},\tau,\tau})_{x_i}^{\mathbf{1}}$, respectively. Explicitly written out, this becomes

$$
\begin{aligned}
P_{2\text{-body}}^{(\mathbf{1})} &= \begin{pmatrix} 1 & & & & \\ & 0 & & & \\ & & 0 & & \\ & & & d^{-2} & d^{-\frac{3}{2}} \\ & & & d^{-\frac{3}{2}} & d^{-1} \end{pmatrix}, \\[2em]
P_{2\text{-body}}^{(\tau)} &= \begin{pmatrix} 0 & & & & \\ & 1 & & & \\ & & 1 & & \\ & & & d^{-1} & -d^{-\frac{3}{2}} \\ & & & -d^{-\frac{3}{2}} & d^{-2} \end{pmatrix}.
\end{aligned}
\quad (2)
$$

One can easily check that $P_{2\text{-body}}^{(\mathbf{1})} + P_{2\text{-body}}^{(\tau)} = \mathbb{1}$, where $\mathbb{1}$ is the identity matrix.

We can now write down the golden chain Hamiltonian as the sum of the projection operators $P_{2\text{-body},i}^{(\tau)}$, $H = J_2 \sum_{i=1}^{L} P_{2\text{-body},i}^{(\tau)}$, where the projector $P_{2\text{-body},i}^{(\tau)}$ assigns a positive energy if the anyons $i$ and $i + 1$ are in the $\tau$ channel. In the original golden chain paper,[2] it was shown numerically that this model is critical for either sign of the interaction. Moreover, the central charge was determined via the entanglement entropy, resulting in $c = 7/10$ and $c = 4/5$ for antiferromagnetic ($J_2 = 1$) and ferromagnetic ($J_2 = -1$) interactions, respectively. Exact diagonalization of the model showed that for antiferromagnetic interactions, the low-lying part of the spectrum can be described in terms of the minimal model $\mathcal{M}_{4,5}$, describing the tricritical Ising model. The critical model describing the ferromagnetic system is that of the $Z_3$ parafermions.

It was subsequently realized that the golden chain Hamiltonian can, in fact, be obtained from an exactly solvable model, a
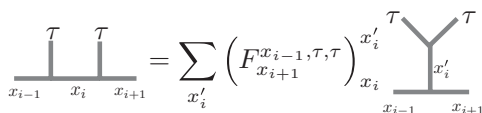
FIG. 3. The $F$ transformations needed for the three-body interaction.

particular version of the RSOS models.[8] These models exhibit various ordered phases, separated by critical points. It is to these critical points that the golden chain can be mapped. As a result, one can obtain information about the critical theory of the golden chain by studying the critical behavior of the RSOS models. We discuss these RSOS models and their connection to the anyonic chain Hamiltonians in more detail in the next section.

### B. Competing interactions

Having introduced the golden chain Hamiltonian, in which the anyons interact via a two-body nearest-neighbor interaction, we now consider the effect of introducing a three-body interaction, which was first considered in Ref. 3.

It is well known that if one adds a three-body term (with large-enough coupling) to the $S = 1/2$ Heisenberg antiferromagnet, a gap opens, and one enters the Majumdar-Ghosh (MG) phase.[22,23] The phase diagram of the Heisenberg chain with competing nearest-neighbor two- and three-body interactions is rather rich. Similarly, it was expected that the phase diagram of the golden chain with competing two- and three-body interactions is rich as well. This model was studied in Ref. 3, indeed finding an interesting phase diagram (see Fig. 4), which we briefly review below, after introducing the details of the three-body interaction.

In order to find the fusion channel of three neighboring anyons, we first have to perform two $F$ transformations, after which this fusion channel is explicit. One can then project onto the desired channel and go back to the original basis. This was explained in detail in Ref. 20. The schematics of the basis transformation is given in Fig. 3.

The three-body interaction depends on four labels $(x_{i-1}, x_i, x_{i+1}, x_{i+2})$. To give the interaction matrix, we use the following basis: $\{(\mathbf{1}, \tau, \tau, \mathbf{1}); (\mathbf{1}, \tau, \mathbf{1}, \tau), (\mathbf{1}, \tau, \tau, \tau); (\tau, \mathbf{1}, \tau, \mathbf{1}), (\tau, \tau, \tau, \mathbf{1}); (\tau, \mathbf{1}, \tau, \tau), (\tau, \tau, \mathbf{1}, \tau), (\tau, \tau, \tau, \tau)\}$. In this basis, the three-body projectors take the following form:

$$P^{(\mathbf{1})}_{\text{3-body}} = \begin{pmatrix} 1 & & & & & & & \\ & 0 & 0 & & & & & \\ & 0 & 0 & & & & & \\ & & & 0 & 0 & & & \\ & & & 0 & 0 & & & \\ & & & & & d^{-2} & d^{-2} & -d^{-\frac{5}{2}} \\ & & & & & d^{-2} & d^{-2} & -d^{-\frac{5}{2}} \\ & & & & & -d^{-\frac{5}{2}} & -d^{-\frac{5}{2}} & d^{-3} \end{pmatrix},$$

$$P^{(\tau)}_{\text{3-body}} = \begin{pmatrix} 0 & & & & & & & \\ & 1 & 0 & & & & & \\ & 0 & 1 & & & & & \\ & & & 1 & 0 & & & \\ & & & 0 & 1 & & & \\ & & & & & d^{-1} & -d^{-2} & d^{-\frac{5}{2}} \\ & & & & & -d^{-2} & d^{-1} & d^{-\frac{5}{2}} \\ & & & & & d^{-\frac{5}{2}} & d^{-\frac{5}{2}} & 2d^{-2} \end{pmatrix}. \quad (3)$$

In terms of these projectors, the most general interaction we can write down takes the form

$$H_{J_2, J_3} = \sum_{i=1}^{L} \cos\theta\, P^{(\tau)}_{\text{2-body}, i} + \sin\theta\, P^{(\tau)}_{\text{3-body}, i}. \quad (4)$$

In this equation, the three-body projectors act on the quadruples $(x_{i-1}, x_i, x_{i+1}, x_{i+2})$, while the two-body projectors act on triples $(x_{i-1}, x_i, x_{i+1})$. Moreover, we assume periodic boundary conditions, $x_{i+L} = x_i$, and we introduced the couplings $J_2 = \cos\theta$ and $J_3 = \sin\theta$.

### C. Phase diagram of the $J_2 - J_3$ model

We now briefly describe the phase diagram of the $J_2 - J_3$ model as a function of the angle $\theta$. For more details, we refer to Refs. 3 and 24. The phase diagram of this model is shown in Fig. 4.

The angle $\theta = 0$ corresponds to the original two-body golden chain model, which is critical and described by the tricritical Ising model. For a finite range of both positive and negative angles, this behavior persists, so we have an extended range of critical behavior. At the angle given by $\tan\theta = 1/\varphi$, with both the two- and three-body interactions antiferromagnetic, there is a phase transition to a gapped phase. In this gapped phase, the ground state is twofold degenerate, with all the ground states occurring at zero momentum. It turns out that at the transition point, which is described by the $Z_3$ parafermion theory, a nonlocal symmetry, dubbed topological symmetry, is broken.



FIG. 4. (Color online) Phase diagram of the $J_2 - J_3$ model; $J_2 = \cos\theta$, $J_3 = \sin\theta$.

The critical phase around $\theta = 0$ also gives way for a gapped phase if $\theta$ is decreased, namely around $\theta \approx -0.472\pi$. In the resulting gapped phase, both the spatial and topological symmetries are broken, giving rise to four (dimerized) ground states. This phase is the anyonic equivalent of the MG phase in spin-$\frac{1}{2}$ chains with a purely three-body interaction. The phase transition from the tricritical Ising region to the MG-like phase is described by the tetracritical Ising model.

The critical behavior at $\theta = \pi$, the original golden chain with ferromagnetic interactions, is described in terms of the $Z_3$ parafermions (the critical behavior of the three-state Potts model). This point is part of an extended critical region, which extends all the way to the gapped phase in the region when both couplings are antiferromagnetic. This end point of that gapped phase is around $\theta \approx 0.316\pi$.

The other end point of the extended critical region containing the point $\theta = \pi$ is marked by a first-order transition located at $\theta \approx 1.075\pi$ to a sliver of an incommensurate region, which quickly gives way to an extended critical region. This region has low-lying states at momenta $K = 0, \pi/2, \pi, 3\pi/2$ and was therefore dubbed the $Z_4$ phase. This phase has a transition to the MG phase around $\theta \approx 1.38\pi$.

We close this quick walk through the phase diagram by noting that there are two special points which lie in the gapped phases, namely at $\tan\theta = \varphi/2$ and $\theta = 3\pi/2$. At these special points, the ground states of the gapped phases are exactly degenerate (as opposed to exponentially degenerate with system size), and moreover, one can obtain these ground states explicitly. For more details about the phase diagram and its peculiarities, we refer to Refs. 3 and 24.

In this paper, we mainly concentrate on a special angle, given by $\tan\theta = 1/\varphi$, which corresponds to (on the one hand) the transition between the extended critical region at antiferromagnetic two-body interactions and the gapped phase obtained by introducing the antiferromagnetic three-body interaction. Upon changing the sign of the Hamiltonian, one ends up in the extended $Z_4$ critical region. We show in the next section that, by making use of the integrable structure at $\theta = 0$, one can show that the $J_2 - J_3$ model is also integrable at $\tan\theta = 1/\varphi$. We confirm that the critical point at $\tan\theta = 1/\varphi$ (with both couplings positive) is indeed described by the $Z_3$ parafermions. In addition, we show that for both couplings negative, the critical theory describing the model is that of the Gepner parafermions related to su(3)$_2$.[25] This latter integrable point lies in an extended critical region. Because there are no relevant operators in the same symmetry sector as the ground state, this whole critical region is described by the same critical theory as the one we found at the integrable point.

### D. Anyonic chains of su(2)$_k$ anyons

In this section, we describe the generalization of the golden chain, where the Fibonacci anyons are replaced by more general types of anyons. These more general anyons are of the type which is dubbed su(2)$_k$, where $k$ is a positive integer. For arbitrary $k$, this anyon theory has $k + 1$ types of anyons, which can be labeled in terms of an "angular momentum" $l$, which takes the values $l = 0, \frac{1}{2}, \ldots, \frac{k}{2}$. For our present purposes, we are mainly interested in the fusion rules of these anyons and

the associated $F$ symbols, which are necessary to construct the Hamiltonians of interacting anyons of this type.

The fusion rules of the su(2)$_k$ anyons are derived from the tensor products of spin representations of SU(2). These have to be modified to take into account that in the anyon model there is a highest angular momentum. This generalization reads as follows. The fusion of two anyons of type $j_1$ and $j_2$ is

$$j_1 \times j_2 = \sum_{j_3 = |j_1 - j_2|}^{\min(j_1 + j_2, k - j_1 - j_2)} j_3, \qquad (5)$$

where the sum is either over the integers or half integers. The only difference between the tensor product rules for SU(2) spins is the upper bound. In particular, the case of the Fibonacci anyons corresponds to $k = 3$. In general, this theory has four anyons, $l = 0, 1/2, 1, 3/2$, but because $k = 3$ is odd, one can restrict oneself to the integer subset (see Ref. 20 for details). This integer subset was written as $\{\mathbf{1}, \tau\}$ in the previous sections.

The model one now considers is the model where the constituent anyons are the $l = \frac{1}{2}$ anyons of su(2)$_k$. The Hilbert space consists of all labelings of the fusion tree in Fig. 1, but with the $\tau$ particles replaced by the $l = \frac{1}{2}$ anyons, and at the vertices the fusion rules in Eq. (5) have to be satisfied. The construction of the interaction matrices, for both the two-body and three-body interactions, is identical to the construction in the Fibonacci case. The only thing which has to be changed is the $F$-matrix elements. Symbolically, we can write the elements of the resulting projection matrices in the same way:

$$\left(P^{(1)}_{\text{2-body},i}\right)^{x_{i-1},\tilde{x}_i,x_{i+1}}_{x_{i-1},x_i,x_{i+1}} = \left(F^{x_{i-1},\frac{1}{2},\frac{1}{2}}_{x_{i+1}}\right)^{\tilde{x}_i}_1 \left(F^{x_{i-1},\frac{1}{2},\frac{1}{2}}_{x_{i+1}}\right)^1_{x_i}, \qquad (6)$$

$$\left(P^{(1/2)}_{\text{3-body},i}\right)^{x_{i-1},\tilde{x}_i,\tilde{x}_{i+1},x_{i+2}}_{x_{i-1},x_i,x_{i+1},x_{i+2}} = \sum_{x'_i,x''_i} \left(F^{x_{i-1},\frac{1}{2}}_{\tilde{x}_{i+1}}\right)^{\tilde{x}_i}_{x''_i} \left(F^{x_{i-1},x''_i,\frac{1}{2}}_{x_{i+2}}\right)^{\tilde{x}_{i+1}}_{1/2}$$
$$\times \left(F^{x_{i-1},x'_i,\frac{1}{2}}_{x_{i+2}}\right)^{1/2}_{x_{i+1}} \left(F^{x_{i-1},\frac{1}{2},\frac{1}{2}}_{x_{i+1}}\right)^{x'_i}_{x_i}. \qquad (7)$$

Here, we wrote the projectors onto the spin-1 and spin-$\frac{1}{2}$ channels for the two- and three-body interactions, respectively. The $F$ matrices themselves can be obtained from the explicit expressions, which were derived in Ref. 21. The Hamiltonian for general $k$ now reads

$$H_{J_2 - J_3} = \sum_i \cos\theta \, P^{(1)}_{\text{2-body},i} + \sin\theta \, P^{(1/2)}_{\text{3-body},i}, \qquad (8)$$

where the $k$ dependence is hidden in the detailed form of the projectors and, of course, in the Hilbert space itself.

The phase diagram of the general $k$ model has the same structure as the phase diagram for $k = 3$ in Fig. 4. The extended critical region around $\theta = 0$ is described by the minimal model $\mathcal{M}_{k+1,k+2}$, the $k$-critical Ising model. The critical phase around $\theta = \pi$ is described by the $Z_k$ parafermions (we refer to Ref. 26 for a description of this CFT). At angles $\theta = 0, \pi$, this follows from the integrability of the RSOS model.[2]

We introduce the notation $d_k = 2\cos[\pi/(k + 2)]$ for the quantum dimension of the spin-$\frac{1}{2}$ anyon of the su(2)$_k$ anyon model. Below, we show that the angles given by $\tan\theta = (d_k^2 - 1)/d_k^2$ are special because we can obtain the critical behavior by mapping the model to a new integrable generalization of the

RSOS model. For the resulting $\theta$ in the range $0 \leqslant \theta \leqslant \pi/2$, this integrable point is the transition from the extended critical region to a gapped phase. From numerics, it was already obtained that this critical behavior is described by the $Z_k$ parafermion theory.[3] Below, we show that this indeed follows by exactly solving the model. The opposite point lies within the so-called $Z_4$ critical region, with low-lying states at the momenta $K = 0, \pi/2, \pi, 3\pi/2$. For this critical region, the numerical results were less clear, but our analysis of the integrable 2D classical statistical mechanics model, which we introduce in this paper, shows that the CFT description of this phase is in terms of a diagonal coset model, namely $\frac{su(2)_1 \times su(2)_1 \times su(2)_{k-2}}{su(2)_k}$. For $k = 3$, this model reduces to the $su(3)_2$ parafermion CFT. Bordering this extended critical phase is the analog of the MG phase around $\theta = 3\pi/2$, which also borders the extended critical phase around $\theta = 0$. The phase transition between the latter two is described by the $k + 1$-critical Ising model.

## III. CONNECTION WITH 2D STATISTICAL MECHANICS MODELS

### A. Integrability of the golden chain model

In the original paper,[2] it was pointed out that the golden chain Hamiltonian can be solved exactly by mapping it onto the RSOS model, which was exactly solved by ABF[8] by means of the CTM method.[9] In particular, the two-body terms $P^{(1)}_{2\text{-body},i}$ in the Hamiltonian at $\theta = 0$, $H_{J_2=1,J_3=0} = \sum_{i=1}^{L} P^{(1)}_{2\text{-body},i}$, can be related to generators of the Temperley-Lieb algebra $e(i)$, namely $e(i) = d_k(\mathbb{1} - P^{(1)}_{2\text{-body},i})$.

The Temperley-Lieb algebra generators satisfy the relations

$$
\begin{aligned}
e^2(i) &= d_k \, e(i), \\
e(i)e(i \pm 1)e(i) &= e(i), \\
[e(i), e(j)] &= 0 \quad \text{for } |i - j| \geqslant 2.
\end{aligned}
\tag{9}
$$

The action of the Temperley-Lieb generators on the local degrees of freedom labeling the states in the Hilbert space can be written, following Pasquier,[27] as

$$
e(i)|x_{i-1}, x_i, x_{i+1}\rangle = \sum_{x_i'} \left[e(i)^{x_{i+1}}_{x_{i-1}}\right]^{x_i'}_{x_i}|x_{i-1}, x_i', x_{i+1}\rangle, \tag{10}
$$

$$
\left[e(i)^{x_{i+1}}_{x_{i-1}}\right]^{x_i'}_{x_i} = \delta_{x_{i-1}, x_{i+1}} \sqrt{\frac{S_{0,x_i} S_{0,x_i'}}{S_{0,x_{i-1}} S_{0,x_{i+1}}}}, \tag{11}
$$

where $S_{i,j}$ are the elements of the modular $S$ matrix of the $su(2)_k$ CFT, which are labeled by $i, j = 0, 1/2, \ldots, k/2$, corresponding to the different type of anyons in $su(2)_k$ theory. Explicitly, one has

$$
S_{i,j} = \sqrt{\frac{2}{k+2}} \sin\left(\frac{(2i+1)(2j+1)\pi}{k+2}\right). \tag{12}
$$

We can write down plaquette weights, or $R$-matrix elements of the corresponding 2D classical statistical mechanics model,
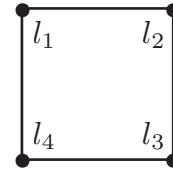


FIG. 5. The plaquette weight $W(l_1, l_2, l_3, l_4)$, which in the anisotropic limit ($u \to 0$) gives rise to the two-body Hamiltonian $H_{J_2=1,J_3=0}$.

in terms of the $e(i)$ and the identity operator $\mathbb{1}$ as follows:

$$
\begin{aligned}
R_i(u)^{\vec{x}'}_{\vec{x}} &= \left(\frac{\sin\left(\frac{\pi}{k+2} - u\right)}{\sin\left(\frac{\pi}{k+2}\right)} \mathbb{1}^{\vec{x}'}_{\vec{x}} + \frac{\sin(u)}{\sin\left(\frac{\pi}{k+2}\right)} e(i)^{\vec{x}'}_{\vec{x}}\right) \\
&\equiv \left(\prod_{j \neq i} \delta_{x_j', x_j}\right) W(x_{i-1}, x_i', x_{i+1}, x_i), \\
e(i)^{\vec{x}'}_{\vec{x}} &= \left(\prod_{j \neq i} \delta_{x_j', x_j}\right) \left[e(i)^{x_{i+1}}_{x_{i-1}}\right]^{x_i'}_{x_i}, \\
\mathbb{1}^{\vec{x}'}_{\vec{x}} &= \prod_j \delta_{x_j', x_j}.
\end{aligned}
\tag{13}
$$

The subscript $i$ on the $R$-matrix labels the plaquette on which it acts, while the argument $u$ is the so-called fugacity, and $W(x_{i-1}, x_i', x_{i+1}, x_i)$ gives the weight of an elementary plaquette shown in Fig. 5. The above $R$ matrix can be shown to satisfy the Yang-Baxter equation,

$$
R_j(u)R_{j+1}(u+v)R_j(v) = R_{j+1}(v)R_j(u+v)R_{j+1}(u), \tag{14}
$$

by making use of the Temperley-Lieb algebra relations for the $e(i)$ in Eq. (9).

From the $R$ matrix, one can construct the "two-row" transfer matrix (see Fig. 6)

$$
T(u) = \prod_j R_{2j+1}(u) \prod_j R_{2j}(u), \tag{15}
$$

which has a role of a discrete time-evolution operator for the corresponding 1D quantum system. The time-evolution operator acts on a Hilbert space, which is spanned by vectors $(\ldots, l_{2j-1}, l_{2j}, l_{2j+1}, \ldots)$. For the golden chain model, this Hilbert space coincides with that given in Fig. 1. We note that in making the connection between the 2D statistical mechanics model and the 1D quantum Hamiltonian, we have rotated the plaquettes by $45°$, or the time runs from the southwest to
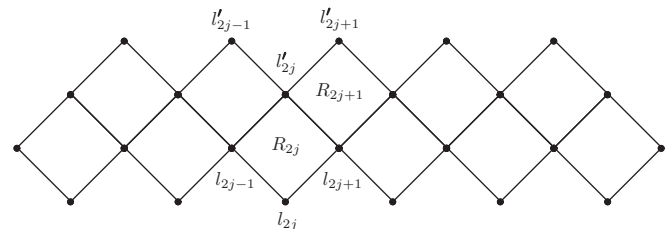


FIG. 6. Two-row transfer matrix, which plays a role of the discrete time-evolution operator for the corresponding 1D quantum system. The transfer matrix acts on the Hilbert space spanned by vectors $(\ldots, l_{2j-1}, l_{2j}, l_{2j+1}, \ldots)$. (Imaginary) time runs vertically.

northeast corner of the plaquette. In addition, we consider a two-row transfer matrix in order that in one discrete time step all heights can evolve. This allows for the possibility to obtain a translationally invariant Hamiltonian. The following calculation shows that this is indeed the case.

If $R_i(u)$ satisfies the Yang-Baxter equation, it follows that the $T$'s at different parameters $u$ commute, allowing one to construct a Hamiltonian which can be solved exactly. In particular, one writes $T(u) = e^{-uH+o(u^2)}$, which gives rise to the Hamiltonian

$$H = -\frac{d \ln T(u)}{du}\bigg|_{u=0} = -\sum_i \frac{1}{R_i(u=0)} \frac{dR_i(u)}{du}\bigg|_{u=0}. \quad (16)$$

Applying this construction to the $R$ matrix defined above, one obtains

$$H = \frac{2}{\tan[\pi/(k+2)]} \sum_i \left( \frac{1}{2} - \frac{1}{d_k} e(i) \right)$$
$$= \frac{2}{\tan[\pi/(k+2)]} \sum_i \left( P^{(1)}_{2\text{-body},i} - \frac{1}{2} \right), \quad (17)$$

which is, up to a *positive* scale factor and an overall shift, equal to the golden chain Hamiltonian, $H_{J_2=1,J_3=0}$.

We now focus our attention on the RSOS model we referred to at the beginning of this section. The model consists of height variables (simply called "heights") located at the vertices of the square lattice. The heights can take the values $l = 1, 2, \ldots, r-1$, where $r$ is an arbitrary integer. We already noted that the heights correspond to the different type of anyons, $0, 1/2, \ldots, k/2$, where $k = r - 2$. The connection with the anyon Hamiltonian becomes complete by the following identification: $r \equiv k + 2$, and $l_i \equiv 2x_i + 1$, where $l_i$ is the value of the height at the vertex $i$.

The heights have to satisfy the constraint that they differ by one if they are nearest neighbors. Weights are assigned to the different types of plaquettes, which we introduce below.

This model can be solved for a two-parameter family of weights, namely for the parameter $u$ and an additional parameter $p$. This parameter $p$ is the parameter which drives a phase transition, located at $p = 0$. The golden chain is related to the RSOS model at this critical point.

We now briefly describe the weights of the RSOS model in terms of the parameters[28] $\eta$ (which is related to $r$; see below), $u$, and $p$. There are six different arrangements of heights around a plaquette, as shown in Fig. 7. The corresponding weights are given in terms of elliptic functions as follows:

$$\alpha_l(u) = \frac{h(2\eta - u)}{h(2\eta)}, \quad \beta_l(u) = \frac{h(u)}{h(2\eta)} \frac{[h(w_{l-1})h(w_{l+1})]^{1/2}}{h(w_l)},$$
$$\gamma_l(u) = \frac{h(w_l + u)}{h(w_l)}, \quad \delta_l(u) = \frac{h(w_l - u)}{h(w_l)}, \quad (18)$$

where $w_l = 2\eta l$. The function $h(u)$ is given in terms of elliptic theta functions, with argument $u$ and modulus $\tilde{k} = m^2$, namely $h(u) = H(u)\Theta(u)$. The functions $H(u)$ and $\Theta(u)$ can be expressed in terms of the $\theta$ functions $\theta_1$ and $\theta_4$, in particular, $H(u) = \theta_1(\frac{u\pi}{2K(m)}, p)$ and $\Theta(u) = \theta_4(\frac{u\pi}{2K(m)}, p)$, where $K(m)$ is the complete elliptic integral of the first kind. The parameter $\eta$ is given in terms of $K$ and $r$, namely $\eta = K/r$. Furthermore, $p$ can be expressed in terms of $m$ as $p = \exp[-\pi K'(m)/K(m)]$,
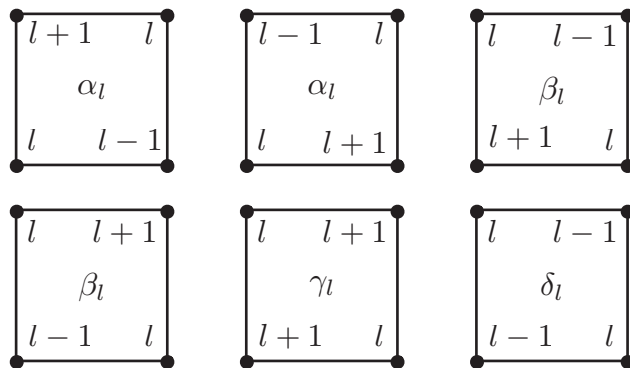


FIG. 7. Six height configurations occurring in the RSOS model.

where $K'(m) = K(1 - m)$. Using the product expansions of the elliptic $\theta$ functions, one can write

$$h(u) = 2p^{1/4} \sin\left(\frac{\pi u}{2K(m)}\right) \prod_{n=1}^{\infty} \left[1 - 2p^n \cos\left(\frac{\pi u}{K(m)}\right) + p^{2n}\right]$$
$$\times (1 - p^{2n})^2. \quad (19)$$

Note that we suppressed the dependence of the weights in Eq. (18) on $p$. We refer to chapter 15 of Ref. 9, where the properties of the elliptic functions used in this paper are analyzed. It was shown in Ref. 8 that the weights given in Eq. (18) satisfy the Yang-Baxter equation for all $u$ and $p$.

Two phase transitions (in different regimes for $u$) occur for $p = 0$, which implies that $m = 0$. These two critical points correspond to the integrable point of the golden chain model with $\tan\theta = 0$ (i.e., the angles $\theta = 0, \pi$ of the $J_2 - J_3$ model). Thus, to relate the weights in Eq. (18) at the critical point to the plaquette weights obtained from the golden chain model, we take the limit $\lim_{p\to 0} h(u_1)/h(u_2) = \sin(u_1)/\sin(u_2)$, where we used that $K(0) = \pi/2$.

Using this limit, one finds, at the critical point, that

$$\alpha_l = \frac{\sin\left(\frac{\pi}{k+2} - u\right)}{\sin\left(\frac{\pi}{k+2}\right)},$$
$$\beta_l = \frac{\sin(u)}{\sin\left(\frac{\pi}{k+2}\right)} \frac{\left[\sin\left(\frac{(l-1)\pi}{k+2}\right)\sin\left(\frac{(l+1)\pi}{k+2}\right)\right]^{1/2}}{\sin\left(\frac{l\pi}{k+2}\right)}, \quad (20)$$
$$\gamma_l = \frac{\sin\left(\frac{l\pi}{k+2} + u\right)}{\sin\left(\frac{l\pi}{k+2}\right)}, \quad \delta_l = \frac{\sin\left(\frac{l\pi}{k+2} - u\right)}{\sin\left(\frac{l\pi}{k+2}\right)},$$

which are identical to those obtained from Eq. (13).

The last statement can be verified by considering the explicit form of the $R$ matrix in Eq. (13). The $\alpha$-type plaquettes are obtained from the first term in Eq. (13), when $x_{i-1} \neq x_{i+1}$. The $\beta$ plaquettes are the "off-diagonal" terms, with $x_i \neq x_i'$, which can occur if $x_{i-1} = x_{i+1}$. Only the second term in Eq. (13) contributes to these plaquettes. Finally, the plaquettes of types $\gamma$ and $\delta$ (which are diagonal, but also have $x_{i-1} = x_{i+1}$) receive contributions from both terms in Eq. (13).

Details of the connection between the critical behavior of the golden chain can be found in the original paper.[2] For details of the various phases of the RSOS model, we refer to Refs. 8 and 10. Approaching the critical point $p = 0$

from the positive $p$ side, one finds that the observables of the model, such as the height probabilities (see below), are given in terms of the tricritical Ising model for $u > 0$, and the three-state Potts model for $u < 0$. This establishes the observed critical behavior of the golden chain model.[2] In general, that is, for arbitrary $k$, this generalizes to the $k$-critical Ising model for antiferromagnetic interactions ($u > 0$) and the $Z_k$ parafermions for ferromagnetic ($u < 0$) interactions.

## IV. CONSTRUCTION OF A NEW COMPOSITE HEIGHT MODEL

### A. $R$ matrix for the composite model

To identify a new integrable model, which corresponds to different parameter regimes of the generalized golden chain model ($J_2 - J_3$ model), we use the ideas put forward in two papers by Ikhlef *et al.*[17,18] In these papers, a model closely related to the anyonic chains is studied. Namely, the underlying algebraic structure, the Temperley-Lieb algebra, is the same, but a different representation is chosen. We consider the "anyonic representation" [see Eq. (11)], while Refs. 17 and 18 consider a spin-$\frac{1}{2}$-type representation. An important consequence of this difference in representation is that we were forced to use the CTM method solve the model, as opposed to the Bethe ansatz method,[29] which was used in Refs. 17 and 18.

Below, we introduce a height model which at its critical point reduces to the anyonic chain at the integrable point. However, we also study the ordered phases of our height model.

It was put forward in Ref. 17, that one can use the $R$ matrix in Eq. (13) to construct a composite $R$-matrix $\tilde{R}$, which also satisfies the Yang-Baxter equation.[30] The composite $R$ matrix one has to consider takes the following form:

$$\tilde{R}_j(u,\phi) = R_{2j+1}(u - \phi)R_{2j}(u)R_{2j+2}(u)R_{2j+1}(u + \phi), \quad (21)$$

where we introduced an additional parameter $\phi$, ranging over $0 \leqslant \phi \leqslant \pi/2$. It can easily be shown that the $R$ matrix (21) satisfies the Yang-Baxter equation. The only ingredient needed to show this is that the original $R$ matrix satisfies the Yang-Baxter equation itself. In what follows, we focus on the case $\phi = \pi/2$, but we stress that the $R$ matrix in Eq. (21) satisfies the Yang-Baxter equation for all values of $\phi$. At $\phi = \pi/2$, the composite $R$ matrix leads to particularly interesting points of the $J_2 - J_3$ Hamiltonian, namely the critical point between the "Haldane gap" phase and the extended AFM critical region. The opposite point (considered in Refs. 17 and 18 in the different representation) lies within the $Z_4$ critical region.

We now describe in some detail how to obtain the Hamiltonian of the $J_2 - J_3$ model, by taking the "anisotropic limit." We start by expanding the composite matrix $\tilde{R}_i(u,\phi)$ explicitly [using the notation $\gamma = \pi/(k + 2)$ and $e_i = e(i)$],

$$
\begin{aligned}
\sin^4&(\gamma)\tilde{R}_i(u,\phi) \\
&= -[\sin(\gamma - u)^2 \sin(\phi + \gamma - u) \sin(\phi - \gamma + u)]\mathbb{1} - [\sin(u) \sin(\gamma - u) \sin(\phi + \gamma - u) \sin(\phi - \gamma + u)](e_{2i} + e_{2i+2}) \\
&\quad + \tfrac{1}{2} \sin(u) \sin(\gamma - u)\{1 + 2\cos(2\phi) - \cos(2\gamma) - \cos[2(\gamma - u)] - \cos(2u)\}e_{2i+1} \\
&\quad + [\sin(u) \sin(\gamma - u) \sin(\phi - u) \sin(\phi - \gamma + u)](e_{2i}e_{2i+1} + e_{2i+2}e_{2i+1}) \\
&\quad + [\sin(u) \sin(\gamma - u) \sin(\phi + u) \sin(\phi + \gamma - u)](e_{2i+1}e_{2i} + e_{2i+1}e_{2i+2}) \\
&\quad - \sin(u)^2 \sin(\phi + \gamma - u) \sin(\phi - \gamma + u)e_{2i}e_{2i+2} + \sin(u)^2 \sin(\phi - u) \sin(\phi - \gamma + u)e_{2i}e_{2i+2}e_{2i+1} \\
&\quad + \sin(u)^2 \sin(\phi + u) \sin(\phi + \gamma - u)e_{2i+1}e_{2i}e_{2i+2} - \sin(u)^2 \sin(\phi + u) \sin(\phi - u)e_{2i+1}e_{2i}e_{2i+2}e_{2i+1}. \quad (22)
\end{aligned}
$$

We note that the coefficients of the terms $e_{2i}e_{2i+1}e_{2i+2}$ and $e_{2i+2}e_{2i+1}e_{2i}$ are zero.

As we explained in the previous section, one can construct a Hamiltonian related to this $R$ matrix via the two-row transfer matrix $T(u) = \prod_j R_{2j+1}(u) \prod_j R_{2j}(u) = e^{-uH+o(u^2)}$ by taking the anisotropic limit [Eq. (16)]. Applying this procedure to the composite $R$ matrix $\tilde{R}_i(u,\phi)$, one sees that in the two-row transfer matrix (see Fig. 6), one has to change $R$ to $\tilde{R}$. Consequently, it is not obvious that the procedure yields a translationally invariant Hamiltonian. Applying the procedure, one obtains

$$
\begin{aligned}
H = \sum_i &\left( \frac{2\cos(2\gamma) - \cos(2\phi) - 1}{2\sin(\gamma + \phi)\sin(\gamma - \phi)} \right)\mathbb{1} - \frac{1}{\sin(\gamma)}(e_i + e_{i+1}) \\
&+ \frac{\sin(\phi)}{\sin(\gamma)\sin(\phi + \gamma)\sin(\phi - \gamma)} \\
&\times [\sin(\phi)\cos(\gamma)(e_i e_{i+1} + e_{i+1}e_i) \\
&+ (-1)^i \cos(\phi)\sin(\gamma)(e_i e_{i+1} - e_{i+1}e_i)]. \quad (23)
\end{aligned}
$$

To make the connection with the anyonic chain, we focus on the case $\phi = \pi/2$, which gives (after dropping the irrelevant constant)

$$H = \frac{2}{\sin(2\gamma)} \sum_i -\cos(\gamma)(e_i + e_{i+1}) + (e_i e_{i+1} + e_i e_{i+1}). \quad (24)$$

We note that for $\phi = 0$, we obtain the original golden chain model $H = -\sum_i e_i$. In the case that $0 < \phi < \pi/2$, the term $(e_i e_{i+1} - e_{i+1}e_i)$ has a nonzero coefficient, which gives rise to a non-Hermitian Hamiltonian and breaks the translational invariance.

To relate the Hamiltonian we just obtained from the composite $R$ matrix to that of the $J_2 - J_3$ model, we write the two- and three-body projectors appearing in the $J_2 - J_3$ anyonic Hamiltonian in terms of the Temperely-Lieb generators $e_i$. In general, the projectors of $p$ spin-$\frac{1}{2}$ particles onto the "spin-$p/2$" channel, can be written in terms of the $e_i$.

Explicitly, for two and three particles, one has (see also Refs. [32] and [33])

$$P_{\text{2-body},i}^{(1)} = \mathbb{1} - \frac{1}{d_k}e_i, \quad P_{\text{3-body},i}^{(3/2)} = \mathbb{1} - \frac{d_k}{d_k^2-1}(e_i + e_{i+1})$$
$$+ \frac{1}{d_k^2-1}(e_i e_{i+1} + e_{i+1}e_i), \quad (25)$$

where we remind the reader that $d_k = 2\cos[\pi/(k+2)]$. In the anyonic spin chain the three-body interaction was written in terms of the projector onto the spin-$\frac{1}{2}$ channel, which reads

$$P_{\text{3-body},i}^{(1/2)} = \frac{d_k}{d_k^2-1}(e_i + e_{i+1}) - \frac{1}{d_k^2-1}(e_i e_{i+1} + e_{i+1}e_i). \quad (26)$$

We can now write the $J_2 - J_3$ model in two different ways, namely,

$$H_{J_2-J_3} = \sum_i \cos(\theta)P_{\text{2-body},i}^{(1)} + \sin(\theta)P_{\text{3-body},i}^{(1/2)}, \quad (27)$$

$$H_e = \sum_i \cos(\theta_e)(e_i + e_{i+1}) + \sin(\theta_e)(e_i e_{i+1} + e_{i+1}e_i). \quad (28)$$

By making use of the projectors in Eqs. (25) and (26), we find the following relation between the angles $\theta$ and $\theta_e$:

$$\tan\theta = \frac{(d_k^2-1)\tan\theta_e}{2d_k(1 + d_k\tan\theta_e)}, \quad \tan\theta_e = \frac{(d_k^2-1) - 2d_k^2\tan\theta}{2d_k\tan\theta}. \quad (29)$$

The angle $\theta_e$ for which the model is integrable, $\theta_{e,\text{int}}$, can be read off from Eq. (24) and is given by $\tan\theta_{e,\text{int}} = -1/\cos\gamma = -2/d_k$. This corresponds to the angle $\theta_{\text{int}}$ in the $J_2 - J_3$ model,

$$\tan\theta_{\text{int}} = \frac{d_k^2-1}{d_k^2}. \quad (30)$$

In particular, in the case $u > 0$, we find that the corresponding angle $\theta$ is given by $\theta = \arctan[(d_k^2-1)/d_k^2] + \pi$, that is, when both the two- and three-body interactions are ferromagnetic. When $u < 0$, we have $\theta = \arctan[(d_k^2-1)/d_k^2]$, and both interactions are antiferromagnetic.

### B. Constructing the composite height model

As we described in the previous section for the original golden chain model, we have to consider a more general 2D height model in order to obtain the critical behavior of the $J_2 - J_3$ model at the integrable points. The plaquettes of this new integrable height model, which we introduce below, reduce to the composite $R$ matrix described above at the critical point $p = 0$.

From the construction of the $R$ matrix, we know how to construct the plaquette weights for the composite 2D classical statistical mechanics model from those of the RSOS model described in the previous section. The new plaquettes consist of four plaquettes in the original RSOS model, as depicted in Fig. 8. The model again lives on the square lattice, where both the vertices as well as the middle of the links have a height variable. Two neighboring heights have to differ by one,
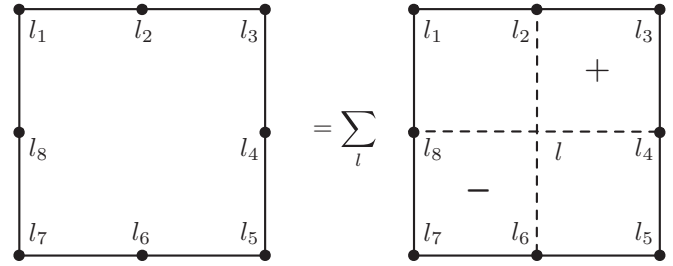


FIG. 8. The plaquette weight $\tilde{W}(l_1,l_2,l_3,l_4,l_5,l_6,l_7,l_8)$ for the composite model in terms of the weights of the RSOS model.

as in the original model. One can think of these plaquettes as composite plaquettes, whose weights depend on the four original plaquettes forming the composite one. The original plaquettes each contribute to the weight of the composite plaquette, but two of the plaquettes have an appropriate "shift," as in the construction of the composite $R$ matrix [see Eq. (21)].

Using the six different types of plaquettes of the RSOS model, it turns out that one can construct 66 different types of composite plaquettes, which are given in Appendix A. Not all the weights of these plaquettes are different. Moreover, they satisfy certain symmetries, in the same way as the original RSOS model. The actual number of different plaquettes depends on the parameter $r$, which determines the number of allowed heights, via $l_i = 1, 2, \ldots, r-1$.

The composite weights $\tilde{W}$ [see Fig. (8)] in term of the RSOS weights have the following form:

$$\tilde{W}(l_{2j-1}, l_{2j}', l_{2j+1}', l_{2j+2}', l_{2j+3}, l_{2j+2}, l_{2j+1}, l_{2j})$$
$$= \sum_l W^-(l_{2j}, l, l_{2j+2}, l_{2j+1})W(l_{2j-1}, l_{2j}', l, l_{2j})$$
$$\times W(l, l_{2j+2}', l_{2j+3}, l_{2j+2})W^+(l_{2j}', l_{2j+1}', l_{2j+2}', l), \quad (31)$$

where $W^\pm(u) = W(u \pm K)$ are the weights of the shifted plaquettes (see Fig. 8). We note that each of the plaquettes forming the composite plaquette is of type $\alpha_l, \beta_l, \gamma_l, \delta_l$, with the appropriate values of $l$, namely,

$$W(l+1,l,l-1,l) = W(l-1,l,l+1,l) = \alpha_l(u),$$
$$W(l,l-1,l,l+1) = W(l+1,l,l-1,l) = \beta_l(u),$$
$$W(l,l+1,l,l+1) = \gamma_l(u),$$
$$W(l,l-1,l,l-1) = \delta_l(u),$$
$$\quad (32)$$

where the explicit expressions of these weights, in terms of the parameters $u$ and $p$, are given in Eq. (18).

Taking into account the quasiperiodic properties of $h(u)$, we have chosen the shift $\phi$ to equal $K$. Again, similar to the RSOS model, we are interested in $p \to 0$ (critical) limit and note that in this limit, $\phi = K = \pi/2$. Due to the symmetry properties of elliptic functions we only need to consider the region $2\eta - K < u < 2\eta + K$, which naturally breaks into two domains according to the sign of $u$ (cf. Ref. [8]):

$$\mathcal{D}_1 : 0 < u < 2\eta + K = (2+r)\eta, \quad (33)$$
$$\mathcal{D}_2 : 2\eta - K = (2-r)\eta < u < 0. \quad (34)$$

The different signs of the fugacity correspond to ferro- ($\mathcal{D}_1$) and antiferromagnetic ($\mathcal{D}_2$) regimes, which in the anisotropic limit give rise to the integrable point of the generalized $J_2 - J_3$ model, for both signs of the interaction.

We have now completely specified our new height model. We employ the CTM method, which is described in the next section, to solve it. The main interest is to calculate local height probabilities in different domains for general $p$, that is, away from criticality. It has been observed that these off-critical ($p \neq 0$) local height probabilities of an integrable lattice model can be mapped to partition functions of the corresponding critical theory ($p = 0$) in a finite box with appropriate boundary conditions.[11] This mapping is realized if one properly relates $p$, which plays the role of temperature, to the finite size $L$ of the critical system. In addition, it has been realized that the local critical probabilities can be written using characters of the underlying CFT.[12] Relying on these observations, we identify CFTs describing critical theories of the generalized anyon model ($p = 0$) in subsequent sections. In particular, we calculate the off-critical local height probabilities and relate them to characters of a CFT, which governs the critical properties of the generalized anyon model (as well as the generalized RSOS model at $p = 0$).

## V. CORNER TRANSFER MATRIX METHOD AND LOCAL HEIGHT PROBABILITIES

### A. Definition of corner transfer matrices

To exactly solve the generalized model, we use the CTM method in analogy to the solution of the RSOS model by ABF.[8] Here, we give a short account of the method and turn the interested reader to literature for more details.[9,34] The object of interest is the local height probability $P_a$, which is the probability for a site to have height $a$. This height probability is given by

$$P_a = \frac{1}{Z} \sum_{\text{configurations}} \left( S_a \prod_{\text{plaquettes}} \tilde{W}(l_{j_1}, l_{j_2}, l_{j_3}, l_{j_4}, l_{j_5}, l_{j_6}, l_{j_7}, l_{j_8}) \right),$$
(35)

where product is over all plaquettes (faces) of the lattice and sum runs over all allowed 2D height configurations, and

$$(S_a)_{\mathbf{l},\mathbf{l'}} = \delta(l_1, a) \prod_{i=1}^{m} \delta(l_i, l_i').$$
(36)

The size of the system is parametrized by $m$, which should not be confused with the $m$ related to the modulus $m^2 = \tilde{k}$ of the $\theta$ functions which appeared in Sec. III. The meaning of the indices $\mathbf{l}, \mathbf{l'}$ of the matrix $S$ will become clear shortly.

The partition function $Z$, which is given by

$$Z = \sum_{\text{configurations}} \prod_{\text{plaquettes}} \tilde{W}(l_{j_1}, l_{j_2}, l_{j_3}, l_{j_4}, l_{j_5}, l_{j_6}, l_{j_7}, l_{j_8}),$$
(37)
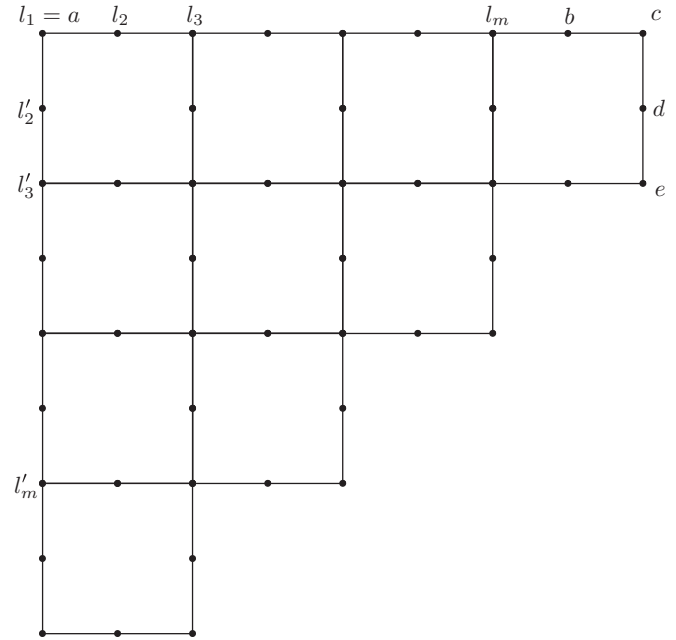
can be expressed as

$$Z = \text{Tr}(ABCD),$$
(38)



FIG. 9. Corner transfer matrix $A$ for finite $m$, constructed using the composite plaquettes. Heights $b,c,d,e$ are the boundary heights fixed by a ground-state pattern chosen.

by introducing CTMs $A, B, C, D$, corresponding to lower-right, upper-right, upper-left, and lower-left quadrants of the lattice [see Fig. 9 and text below for the precise definition of $A, B, C, D$]. These CTMs are analogs of the row-to-row transfer matrix $T$, but instead of adding a row to the lattice, they add a whole corner.

Finally, the local height probability can be written as

$$P_a = \text{Tr}(S_a ABCD)/\text{Tr}(ABCD).$$
(39)

We now have to introduce the notion of *ground states*, which is used extensively in the subsequent analysis. Ground states are those configurations of heights which maximize the summand (or minimize the "energy") in Eq. (37). These ground states depend on $u$ in a way that in different domains of $u$ ($\mathcal{D}_1$ and $\mathcal{D}_2$) different ground-state types exist and they change discontinuously across the boundary between different domains ($u = 0$). These different ground states determine different critical behavior in corresponding domains as we show below.

The CTMs can be expressed using *local* plaquette (face) transfer matrices

$$(U_j)_{\mathbf{l},\mathbf{l'}} = \tilde{W}(l_{2j-1}, l_{2j}', l_{2j+1}', l_{2j+2}', l_{2j+3}, l_{2j+2}, l_{2j+1}, l_{2j})$$
$$\times \prod_{i=1 \neq 2j, 2j+1, 2j+2}^{m} \delta(l_i, l_i'),$$
(40)

$$(V_j)_{\mathbf{l},\mathbf{l'}} = \tilde{W}(l_{2j+1}', l_{2j+2}', l_{2j+3}, l_{2j+2}, l_{2j+1}, l_{2j}, l_{2j-1}, l_{2j}')$$
$$\times \prod_{i=1 \neq 2j, 2j+1, 2j+2}^{m} \delta(l_i, l_i').$$
(41)

Here $j = 1, \ldots, (m+1)/2$, with $m$ odd, and $l_{m+1}, l'_{m+1}, l_{m+2}, l'_{m+2}, l_{m+3}, l'_{m+3}, l_{m+4}$ are boundary heights, which should be fixed to proper ground state values corresponding to a considered domain of $u$. The matrix $U_j$ ($V_j$) adds a plaquette to the lattice in the NE-SW (NW-SE) direction.

Using the definitions in Eqs. (40) and (41), the CTM $A$ can be expressed as

$$A = F_1 F_2, \ldots, F_{(m+1)/2}, \tag{42}$$

where

$$F_j = U_{(m+1)/2} U_{(m-1)/2}, \ldots, U_j. \tag{43}$$

The CTM $A$ (see Fig. 9) has rows and columns, which are labeled by the values of the boundary heights, collected in the vectors $\mathbf{l} = (l_1, l_2, \ldots, l_m)$ and $\mathbf{l'} = (l'_1, l'_2, \ldots, l'_m)$, where $l'_1 = l_1 = a$, because these heights correspond to the same central height. In addition, we use boundary conditions, such that the heights on the four outermost diagonals are fixed to be $b, c, d, e$, respectively.

The CTMs $B, C, D$ are expressed similarly to $A$ by replacing $U_j$ with $V_j$, $U_j^T$, and $V_j^T$, respectively. In general, properties of the CTMs depend on symmetries of weights as well as those of ground states. In what follows, we are interested in infinite lattice limit, $m \to \infty$.

### B. Corner transfer matrices as exponentials

From the Yang-Baxter equation for weights [see Eq. (14)] follows a very important property of corner transfer matrices. In the limit where the lattice size goes to infinity we can write (symbolically) that

$$\lim_{m \to \infty} B\,C = \lim_{n \to \infty} T^n, \tag{44}$$

where $T$ is the row-to-row transfer matrix and $n$ is the number of rows, covering a half plane in the limit $n \to \infty$.

We should note that the above relation is not valid for finite $m$ and $n$, since different boundary conditions are used to calculate left- and right-hand sides of the equation (in fact, even the shapes of the lattices differ). However, in the large $m, n$ limit this difference becomes negligible. The Yang-Baxter equation ensures that the row-to-row transfer matrices with different fugacities commute and, hence, the product $B(u)C(v)$ depends only on the difference $u - v$ (modulus the overall multiplicative factor). Similar equations that involve other corner transfer matrices can be obtained by rotating the lattice in steps of $\pi/2$. Using these properties one can show that the corner transfer matrices have the following form (dropping irrelevant multiplicative factors):[9]

$$\begin{aligned}
A(u) &= Q_1 M_1 e^{-u\mathcal{H}} Q_2^{-1}, \\
B(u) &= Q_2 M_2 e^{u\mathcal{H}} Q_3^{-1}, \\
C(u) &= Q_3 M_3 e^{-u\mathcal{H}} Q_4^{-1}, \\
D(u) &= Q_4 M_4 e^{u\mathcal{H}} Q_1^{-1},
\end{aligned} \tag{45}$$

where the matrices $\mathcal{H}, Q_1, \ldots, Q_4, M_1, \ldots, M_4$ are independent of $u$ and can be chosen to commute with $S_1, \ldots, S_{r-1}$. In addition, the matrices $\mathcal{H}, M_1, \ldots, M_4$ are diagonal.

Using the identity (see Appendix B)

$$A(0) = Q_1 M_1 Q_2^{-1} = \mathbb{1}, \tag{46}$$

we immediately see that

$$A(u) = Q_2 e^{-u\mathcal{H}} Q_2^{-1}, \tag{47}$$

which implies that the diagonal form of the CTM $A$ can be written as an exponential. From Eqs. (39) and (45) we immediately see that

$$P_a = \mathrm{Tr}(S_a M_1 M_2 M_3 M_4) / Tr(M_1 M_2 M_3 M_4). \tag{48}$$

To calculate $M_1 M_2 M_3 M_4$ we need to consider different domains of $u$ separately to find different limiting properties of the CTMs. Here we summarize the properties of the corner matrices near the boundaries of domains $\mathcal{D}_1$ and $\mathcal{D}_2$ (see Appendix B for details), which are required for the calculation. In the domain $\mathcal{D}_1$, in the $u \to 0$ limit we find (upon dropping an irrelevant multiplicative factor)

$$A(u = 0) = C(u = 0) = \mathbb{1}, \tag{49}$$

while in the $u \to (2 + r)\eta$ limit we have

$$B[u = (2+r)\eta] = D[u = (2+r)\eta] = \tilde{V}_1, \tag{50}$$

where we have defined

$$(\tilde{V}_1)_{\mathbf{l}, \mathbf{l'}} = [h(2\eta l_1)]^{1/2} \delta(\mathbf{l}, \mathbf{l'}). \tag{51}$$

Using the above limits for CTMs we can write that

$$A(u = 0)B[u = (2+r)\eta]C(u = 0)D[u = (2+r)\eta] = \tilde{V}_1^2. \tag{52}$$

Substituting Eq. (45) in the above equation we get the following result for the product of the matrices $M_1 M_2 M_3 M_4$, which appear in the expression for the height probability in Eq. (48):

$$M_1 M_2 M_3 M_4 e^{2(2+r)\eta\mathcal{H}} = \tilde{V}_1^2. \tag{53}$$

In the domain $\mathcal{D}_2$, we can show that

$$A(u = 0)B[u = (2-r)\eta]C(u = 0)D[u = (2-r)\eta] = \tilde{V}_1^2 \tag{54}$$

and

$$M_1 M_2 M_3 M_4 e^{2(2-r)\eta\mathcal{H}} = \tilde{V}_1^2. \tag{55}$$

Taking into account relations in Eqs. (53) and (55), the local height probability can be written as

$$P_a = \mathrm{Tr}\big(S_a \tilde{V}_1^2 e^{-2t\eta\mathcal{H}}\big) / \mathrm{Tr}\big(\tilde{V}_1^2 e^{-2t\eta\mathcal{H}}\big), \tag{56}$$

where

$$t = \begin{cases} 2 + r & u \in \mathcal{D}_1, \\ 2 - r & u \in \mathcal{D}_2. \end{cases} \tag{57}$$

### C. Diagonal form of the corner transfer matrix $A$

What is left to do is to find the diagonal form of the CTM $A$ and the matrix $\mathcal{H}$, which is the most involved part of the calculation. The CTMs in Eq. (45) should satisfy quasiperiodic conditions as do the weights, with the period $2iK'$, which implies that elements of $\mathcal{H}$ are integer multiples of $\pi/K'$, $\mathcal{H}_{\mathbf{l},\mathbf{l'}} = \pi N(\mathbf{l})\delta(\mathbf{l},\mathbf{l'})/K'$. Similar to the solution of the RSOS models,[8] we assume that $\mathcal{H}$ does not change discontinuously with $p$, which implies that the integer function $N(\mathbf{l})$ is independent of $p$ and we can derive it in a limit where the composite weights assume a simple form. We can show that (see Appendix C) in the $p \to 1$ limit the weights of the composite model take a particularly simple form and the CTM $A$ can be readily diagonalized. After a fairly lengthy calculation, involving the "conjugate-modulus" (or modular) transformation, the dust settles, and one finds the diagonal form of $A$,

$$A_{\mathbf{l},\mathbf{l'}} = [e^{-u\mathcal{H}}]_{\mathbf{l},\mathbf{l'}} = g_{l_1}^{-1} w^{N(\mathbf{l})/2}\delta(\mathbf{l},\mathbf{l'}), \tag{58}$$

where

$$w = e^{-2\pi u/K'}, \quad g_{l_1} = w^{(2l_1-r)^2/(16r)}, \tag{59}$$

and

$$
\begin{aligned}
N(\mathbf{l})/2 &\equiv \phi(\mathbf{l}) \\
&= \sum_{j=1}^{(m+1)/2} j\left( \frac{|l_{2j+3} - l_{2j-1}|}{4} + \delta_{l_{2j-1},l_{2j+1}}\delta_{l_{2j+1},l_{2j+3}}\delta_{l_{2j},l_{2j+2}} \right),
\end{aligned}
\tag{60}
$$

where sum over $j$ is performed along a line in the 2D lattice (see Fig. 9). Each term in this sum corresponds to the weight of the $j$th plaquette (counted from the central site), times $j$, which is the number of plaquettes on the $j$th diagonal. In the limit $p = 1$, these plaquettes all have the same form, because $A$ is diagonal then, as shown in Appendix C.

### D. Local height probability

We can now collect the results and obtain the local height probabilities $P_a$. Substituting the diagonal form of $A$, Eq. (58) in Eq. (56), we find that

$$P_a = S^{-1}v_a X_m(a;b,c,d,e;x^t). \tag{61}$$

Here we adopted the following definitions:

$$X_m(a;b,c,d,e;q) = \sum_{l_2,\dots,l_m} q^{\phi(\{l\})}, \tag{62}$$

$$v_a = x^{(2-t)(2a-r)^2/(16r)} E(x^a,x^r), \tag{63}$$

$$S = \sum_a v_a X_m(a;b,c,d,e;x^t), \tag{64}$$

$$x = e^{-4\pi\eta/K'}. \tag{65}$$

The function $\phi(\mathbf{l})$ was given in Eq. (60) and the function $E(z,x)$ appears in Jacobi's triple product identity,

$$E(z,x) = \prod_{n=1}^{\infty}(1-x^{n-1}z)(1-x^nz^{-1})(1-x^n). \tag{66}$$

Furthermore, $l_1 = a$ and heights $b,c,d,e$ (see Fig. 9) are the boundary heights, which are to be fixed to the values of a ground state in the domain of $u$ under consideration. We see from Eq. (62) that the partition function as well as the local height probability is expressed as a sum over 1D height configurations, in contrast to 2D configurations in the original formulation [see Eq. (37)]. This property is the consequence of integrability of the model and greatly simplifies calculations.

## VI. PHASES OF THE COMPOSITE HEIGHT MODEL

In this section, we make a start with the exploration of the phase diagram of the composite height model, which is focused on the regions which are related to the anyonic quantum chain. We will give a more detailed description of the various phases of the model in a forthcoming publication.

The phase diagram of the composite height model bears resemblance to the phase diagram of the original RSOS model. We consider the phase diagram as a function of the parameters $u$ and $p$, where the parameter $u$ is related to the anisotropy of the model. Only the sign of this parameter is relevant. The parameter $p$ drives a phase transition between different ordered and disordered phases, as was the case in the RSOS model. We consider the regime $0 \leqslant p \leqslant 1$, which is the one relevant for our purposes.

We start by analyzing the ordered phases by taking either $u > 0$, which we call regime III, or $u < 0$, called regime II. The naming of the regimes follows the nomenclature of ABF. We use the results of the previous section, where we calculated the height probabilities in terms of the functions

$$X_m(a;b,c,d,e;q) = \sum_{l_2,l_3,\dots,l_m} q^{\phi(\mathbf{l})}, \tag{67}$$

where the vector $\mathbf{l}$ has $m + 4$ components, $\mathbf{l} = (a,l_2,\dots,l_m,b,c,d,e)$, which satisfy the constraint $l_i = l_{i-1} \pm 1$, implying that $a + e = 0 \bmod 2$. We repeat the function $\phi(\mathbf{l})$ for convenience,

$$\phi(\mathbf{l}) = \sum_{j=1}^{(m+1)/2} j\left( \frac{|l_{2j+3} - l_{2j-1}|}{4} + \delta_{l_{2j-1},l_{2j+1}}\delta_{l_{2j+1},l_{2j+3}}\delta_{l_{2j},l_{2j+2}} \right). \tag{68}$$

For $0 < p < 1$, the height probabilities are proportional to $X_m(a;b,c,d,e;x^t)$, with $t = 2 + r$ for $u > 0$, and $t = 2 - r$ for $u < 0$.

To find the ground states, we analyze the function $\phi(\mathbf{l})$. The ground states are those configurations which contribute maximally to the partition function. In domain $\mathcal{D}_1$, which has $u > 0$, and $t = 2 + r > 0$, the ground states are given by those configurations which minimize the function $\phi(\mathbf{l})$. For domain $\mathcal{D}_2$, with $u < 0$ and $t = 2 - r < 0$, the function $\phi(\mathbf{l})$ should be maximized instead. As long as $0 < p < 1$, one finds that the arguments about the ground states go through, because $x < 1$. At the critical point ($p \to 0$) we have $x \to 1$; hence, the argument fails and all height configurations contribute equally.

The model is critical when $p \to 0$, and we study the full height probabilities $P_a$, which give the probability that the central height takes the value $a$, depending on the boundary

heights $(b,c,d,e)$ (see Fig. 9). We evaluate these height probabilities, in the case that the boundary heights are such that they belong to a ground-state pattern.

### A. Ground states for $u > 0$ (domain $\mathcal{D}_1$)

Let us start by analyzing the case $u > 0$ and minimize the function $\phi(\mathbf{l})$. In this case, as many plaquettes as possible should give zero contribution to $\phi(\mathbf{l})$. This can be achieved in the following way. First of all, one should have that $l_i = l_{i+4}$, such that the first term within the parentheses in Eq. (68) is zero. There are now two different ways in which one can avoid a contribution from the second term. First, one can set $l_{i+2} = l_i \pm 2$ and $l_{i+1} = l_{i+3} = l_i \pm 1$, where the sign in both equations should be the same. The other possibility is $l_{i+2} = l_i$, while $l_{i+1} = l_i \pm 1$ and $l_{i+3} = l_i \mp 1$, where the signs in the last two equations have to be opposite.

In particular, the vector $\mathbf{l}$ describing the ground states for $0 < p < 1, u > 0$ takes the form (we show the case $r = 7$)

$$(1,2,3,2,1,2,3,2,1,\ldots) \quad (2,3,4,3,2,3,4,3,2,\ldots)$$
$$(3,4,5,4,3,4,5,4,3,\ldots) \quad (4,5,6,5,4,5,6,5,4,\ldots)$$
$$(3,2,1,2,3,2,1,2,3,\ldots) \quad (4,3,2,3,4,3,2,3,4,\ldots)$$
$$(5,4,3,4,5,4,3,4,5,\ldots) \quad (6,5,4,5,6,5,4,5,6,\ldots)$$

for the ground states of the first type. The patterns of the second type are mere translations of the patterns of the first type, and are given by the vectors $\mathbf{l}$ of the form

$$(2,1,2,3,2,1,2,3,2,\ldots) \quad (3,2,3,4,3,2,3,4,3,\ldots)$$
$$(4,3,4,5,4,3,4,5,4,\ldots) \quad (5,4,5,6,5,4,5,6,5,\ldots)$$
$$(2,3,2,1,2,3,2,1,2,\ldots) \quad (3,4,3,2,3,4,3,2,3,\ldots)$$
$$(4,5,4,3,4,5,4,3,4,\ldots) \quad (5,6,5,4,5,6,5,4,5,\ldots).$$

In the limit $p = 1$, the CTM $A$ is diagonal, which gives rise to ground-states patterns which are invariant under translation along the northeast to southwest (NE-SW) diagonal. A particular ground-state pattern for $u > 0$ is displayed in Fig. 10. All the ground states are of the form $(l-1,l,l+1,l,l-1,l,l+1,\ldots)$, or translations of this pattern.

To count the number of different ground states, we note that the ground-state patterns are specified by three consecutive integers. Because the heights can take the values $1,2,\ldots,r-1$, there are $r-3$ possible consecutive integers. By translation, each of these sets of consecutive integers gives rise to four different ground states, for a total of $4(r-3)$ ground states.

We now count the number of different height probabilities, $P_a(b,c,d,e)$, where the boundary condition $(b,c,d,e)$ corresponds to a ground-state pattern. First, we note that $a$, the height of the central site, and $e$ have to have the same parity, $a + e = 0 \mod 2$. For $r$ odd, there are $(r-1)/2$ odd-valued heights and $(r-1)/2$ even-valued heights. In both cases, $a$ can take $(r-1)/2$ values, giving $2(r-1)(r-3)$ different height probabilities. In the case that $r$ is even, there are $r/2$ odd-valued heights and $r/2-1$ even-valued heights. Of the $4(r-3)$ ground-state patterns, $2(r-3)$ have $e$ even and $2(r-3)$ have $e$ odd. Hence, also for $r$ even, the
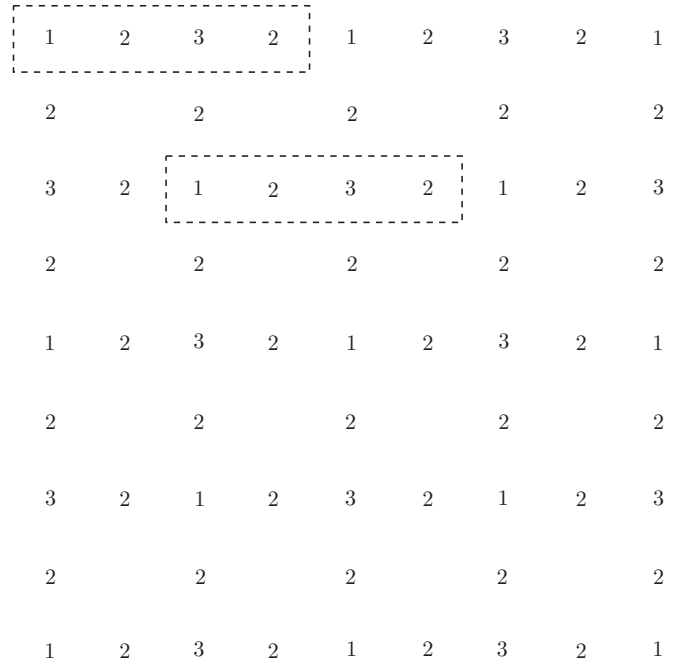


FIG. 10. Ground-state pattern for $u > 0$, which is characterized by the pattern in the dashed boxes.

number of height probabilities to consider is $2(r-1)(r-3)$. These height probabilities are given in terms of the functions $X_m(a;b,c,d,e;q)$, which satisfies the relation (which follows from the symmetry properties of the plaquette weights)

$$X_m(a;b,c,d,e;q) = X_m(r-a;r-b,r-c,r-d,r-e;q).$$
$$(69)$$

This halves the number of independent height probabilities, which is thus given by $(r-1)(r-3)$, or in terms of $k = r-2$, by $k^2 - 1$.

### B. Ground states for $u < 0$ (domain $\mathcal{D}_2$)

We now consider the ground states for $u < 0$ and look for configurations which maximize the function $\phi(\mathbf{l})$. Because $l_i$ and $l_{i+4}$ maximally differ by four, both terms within the parentheses in Eq. (68) can maximally contribute 1. However, in order that the first term contributes for every plaquette, the heights $l_i$ would have to steadily increase or decrease, which is impossible, because the values the $l_i$ can take lie in the range $l_i = 1,2,\ldots,r-1$. The second term inside of the parentheses in Eq. (68) can be 1 for all plaquettes. The only requirement is that $l_{2j-1} = l_{2j+1} = l_{2j+3}$ and $l_{2j} = l_{2j+2} = l_{2j-1} \pm 1$. For $p = 1$, the ground states again are invariant under translations over the NE-SW diagonal. Thus, for $u < 0$, the ground states are given by configurations for which the heights stay as constant as possible; that is, they take the form $(l,l+1,l,l+1,l,\ldots)$, as depicted in Fig. 11 for a typical example.

The number of ground-state patterns is given by the number of consecutive pairs (both increasing and decreasing), that is, $2(r-2)$. We again need the number of height probabilities we
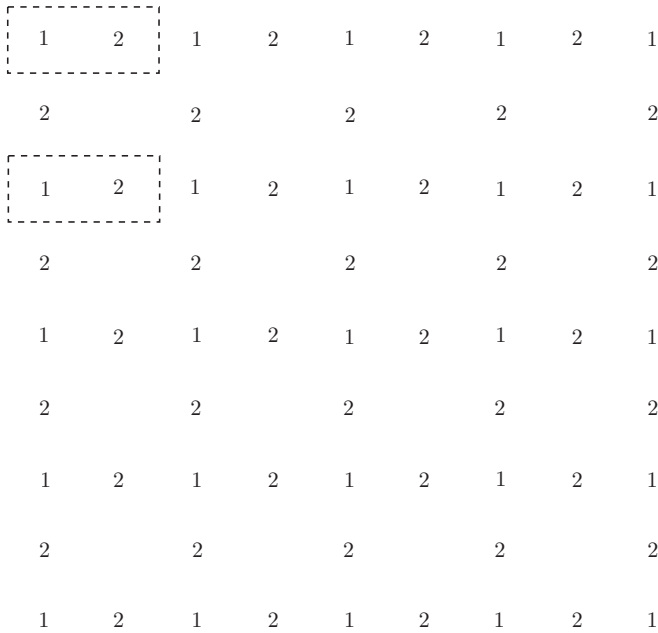
| | | | | | | | | |
|---|---|---|---|---|---|---|---|---|
| 1 | 2 | 1 | 2 | 1 | 2 | 1 | 2 | 1 |
| 2 | | 2 | | 2 | | 2 | | 2 |
| 1 | 2 | 1 | 2 | 1 | 2 | 1 | 2 | 1 |
| 2 | | 2 | | 2 | | 2 | | 2 |
| 1 | 2 | 1 | 2 | 1 | 2 | 1 | 2 | 1 |
| 2 | | 2 | | 2 | | 2 | | 2 |
| 1 | 2 | 1 | 2 | 1 | 2 | 1 | 2 | 1 |
| 2 | | 2 | | 2 | | 2 | | 2 |
| 1 | 2 | 1 | 2 | 1 | 2 | 1 | 2 | 1 |

FIG. 11. Ground-state pattern for $u < 0$, which is formed characterized by the pattern in the dashed boxes.

have to consider, or the number of functions $X_m(a; b,c,d,e; q)$. We only have to specify $(a; d,e)$, because $d$ and $e$ fix the values of $b$ and $c$ in the ground states. There are $2(r - 2)$ pairs $(d,e)$. It turns out that the number of height probabilities is given by $(r - 1)(r - 2)$, irrespective of whether $r$ is even or odd. Thus, there are $(r - 1)(r - 2)/2 = k(k + 1)/2$ independent height probabilities, because of the relation in Eq. (69).

### C. Criticality at $p = 0$

We found the ground states for $u > 0$ and $u < 0$ deep in the ordered regime, namely for $0 < p < 1$, by minimizing or maximizing the function $\phi(\mathbf{l})$, which appears in the height probabilities, as well as the partition function. At the critical point, for $p = 0$ as in the original RSOS model, all configurations contribute, and one has to do a more careful study of the model. In the remainder of this paper, we focus on the full form of the height probabilities, which have a close connection with CFT characters, which allows us to unambiguously identify the critical behavior of the model, for both regimes $u > 0$ and $u < 0$. Because we already established the connection between the composite height model and the anyonic chains, we thereby also explain the critical behavior of the anyonic chains at the integrable point. A more detailed study of the critical behavior of the composite height model will be left for a future publication.

### VII. EVALUATION OF THE HEIGHT PROBABILITIES

We now turn our attention to the evaluation of the height probabilities. We have shown that the probability that the central height takes the value $a$ depends on the boundary condition, which we specified by fixing the boundary heights $(b,c,d,e)$. The height probabilities are governed by the functions $X_m(a; b,c,d,e; q)$ given in Eqs. (67) and (68). We are ultimately interested in the behavior of these functions in the limit $m \to \infty$. In that limit, we can let the boundary heights correspond to the ground-state patterns, which extremize the function $\phi(\mathbf{l})$.

We therefore consider the functions $X_m(a; b,c,d,e; q)$, for all possible values of $(a; b,c,d,e)$ such that the boundary heights $(b,c,d,e)$ are part of a ground-state pattern. In the limit $m \to \infty$, these functions receive contributions from all possible configurations specified by the vectors $\mathbf{l}$. For finite $m$, these functions are finite polynomials in $q$ (or $q^{1/2}$ times such polynomials). The minimal power of $q$ which can occur is zero, while the maximal power is $(m + 1)(m + 3)/8$. We note that these extremal values are not obtained for all choices of $(a; b,c,d,e)$.

In the following sections, we provide explicit expressions for the functions $X_m(a; b,c,d,e; q)$ in the case $r = 5$. We did not yet obtain explicit expressions for $r > 5$, but by analyzing the functions, we unambiguously identified them as the characters of certain conformal field theories. In particular, we checked extensively that in the limit of $m \to \infty$, the functions $X_m(q)$ tend to affine Lie algebra branching functions, or, in other words, characters of the various primary fields in certain coset models. This is precisely the connection we are after, because these coset models describe the behavior of the model at the critical point and hence the critical behavior of the anyonic quantum chains. Before delving into the details, we first state the results here.

For $u > 0$, we find that the functions $X_m(a; b,c,d,e; q)$ tend to the characters of the coset $\frac{\mathrm{su}(2)_1 \times \mathrm{su}(2)_1 \times \mathrm{su}(2)_{k-2}}{\mathrm{su}(2)_k}$, where $k = r - 2$. In the case that $k = 3$, this coset is equivalent to a Gepner parafermion theory[25] based on $\mathrm{su}(3)_2$, explicitly $\frac{\mathrm{su}(3)_2}{u(1)_4 u(1)_{12}}$. The characters of this theory were considered in Ref. 35 in the context of a particular non-Abelian spin-singlet quantum Hall state.[36] The finitizations of the characters considered in Ref. 35 precisely correspond to the functions $X_m(q)$ we obtain from the integrable model we introduced in this paper.

For $u < 0$, one needs to consider the part of the functions $X_m(q)$ with the highest powers of $q$, as explained below. In particular, the functions $q^{(m+1)(m+3)/8} X_m(q^{-1})$ are the functions one needs to consider in the limit $m \to \infty$. We found that they precisely correspond to the characters of the $Z_k$ parafermion theory[26] (which is, for instance, given by the coset $\frac{\mathrm{su}(2)_k}{u(1)_{2k}}$). The characters of this theory can be found in Ref. 37.

For $r = 5$, we have the interesting situation that the finitization of the characters of the $\mathrm{su}(3)_2$ Gepner parafermions, that is, the functions $X_m(q)$, also can be considered as finitized characters of the $Z_3$ parafermions. Because both theories contain Fibonacci particles, one could say that "Fibonacci meets Fibonacci," in the same spirit as "Ising meets Fibonacci,"[6] which establishes a connection between the theories $\mathrm{su}(2)_2$ and $\mathrm{su}(3)_2$, which have Ising and Fibonacci-type fusion rules.

In the following two sections, we provide explicit expressions for the functions $X_m(a; b,c,d,e; q)$, for finite $m$ in the case, $r = 5$. These expressions are such that the limit $m \to \infty$ can be taken explicitly.

The identification of the functions $X_m(a;b,c,d,e;q)$ for all values of $r$ and $(a;b,c,d,e)$ in terms of the CFT characters is the subject of Appendix D, which deals with both cases $u > 0$ and $u < 0$.

### A. Probability amplitudes for $u > 0$

In this section, we give the explicit form of the functions $X_m(a;b,c,d,e,q)$ for those values of $(a;b,c,d,e)$ which correspond to the ground states for $u > 0$ (for $r = 5$). We did not yet prove these results, but we expect that a proof along the lines of the original paper[8] is feasible. Such a proof involves the recursion relations for the functions $X_m(a;b,c,d,e,q)$, which we give in Appendix D [Eq. (D1)].

We start by giving the expressions for finite $m$ and take the limit $m \to \infty$ afterward. We introduce the function $(q)_m = \prod_{k=1}^{m}(1 - q^k)$, for positive integers $m$, and $(q)_0 = 1$, which appears in the definition of the $q$ binomials, or Gaussian polynomials

$$\begin{bmatrix} m \\ n \end{bmatrix} = \begin{cases} \frac{(q)_m}{(q)_n(q)_{m-n}} & \text{for} \quad 0 \leqslant n \leqslant m, \\ 0 & \text{otherwise.} \end{cases} \qquad (70)$$

The precise form of the following function we introduce was inspired by the (finitized) character of the Gepner parafermions associated with $su(3)_2$ (see Ref. 35), as well as the characters for the original RSOS model (see, for instance, Ref. 13). In particular, we introduce

$$y(m; l_2, l_3, l_4; q) = \sum_{a,b \geqslant 0}' q^{\frac{a^2+b^2-ab-a\delta_{l_4,3}-b\delta_{l_4,2}}{2}} \begin{bmatrix} \frac{m+b+\delta_{l_3,1}+\delta_{l_4,3}}{2} \\ a \end{bmatrix}$$
$$\times \begin{bmatrix} \frac{m+a+\delta_{l_2,1}+\delta_{l_3,2}+\delta_{l_4,2}}{2} \\ b \end{bmatrix}, \qquad (71)$$

where we assume that $m$ is an integer, $l_2, l_3 = 1,2$ and $l_4 = 1,2,3,4$. The prime on the sum indicates the constraints that the argument of the $q$ binomials have to be (non-negative) integers. We labeled the function with $l_2, l_3, l_4$, because of the connection with CFT characters, which we describe below (the label $l_1$ can always be chosen as $1$).

We then have the following results

$$X_m(1;2,1,2,3;q) = y\left(\frac{m-1}{2}; 1,1,1;q\right),$$

$$X_m(3;2,1,2,3;q) = y\left(\frac{m-1}{2}; 1,1,3;q\right),$$

$$X_m(2;3,2,3,4;q) = y\left(\frac{m-1}{2}; 1,2,2;q\right),$$

$$X_m(4;3,2,3,4;q) = y\left(\frac{m-1}{2}; 1,2,4;q\right),$$

$$X_m(2;1,2,3,2;q) = y\left(\frac{m-1}{2}; 2,1,2;q\right),$$

$$X_m(4;1,2,3,2;q) = y\left(\frac{m-1}{2}; 2,1,4;q\right),$$

$$X_m(1;2,3,4,3;q) = y\left(\frac{m-1}{2}; 2,2,1;q\right)$$
$$+ q^{\frac{m+1}{4}} y\left(\frac{m-3}{2}; 1,1,1;q\right),$$

$$X_m(3;2,3,4,3;q) = y\left(\frac{m-1}{2}; 2,2,3;q\right)$$
$$+ q^{\frac{m+1}{4}} y\left(\frac{m-3}{2}; 1,1,3;q\right). \qquad (72)$$

We can now rather easily take the limit $m \to \infty$, by using the result

$$\lim_{n \to \infty} \begin{bmatrix} n \\ n' \end{bmatrix} = \frac{1}{(q)_{n'}}.$$

We assume that $m$ is of the form $4p + 3$, with $p$ integer (the case $m = 4p + 1$ is only slightly different). By taking this limit, we find that

$$\lim_{p \to \infty} X_{4p+3}(1;2,1,2,3;q) = c_{\mathbf{1}}^{su(3)_2}(q),$$

$$\lim_{p \to \infty} X_{4p+3}(4;3,2,3,4;q) = \lim_{p \to \infty} X_{4p+3}(4;1,2,3,2;q)$$
$$= \lim_{p \to \infty} X_{4p+3}(1;2,3,4,3;q)$$
$$= c_{\psi}^{su(3)_2}(q), \qquad (73)$$

$$\lim_{p \to \infty} X_{4p+3}(2;3,2,3,4;q) = \lim_{p \to \infty} X_{4p+3}(2;1,2,3,2;q)$$
$$= \lim_{p \to \infty} X_{4p+3}(3;2,3,4,3;q)$$
$$= q^{-\frac{1}{10}} c_{\sigma}^{su(3)_2}(q),$$

$$\lim_{p \to \infty} X_{4p+3}(3;2,1,2,3;q) = q^{-\frac{1}{10}} c_{\rho}^{su(3)_2}(q).$$

Here, the functions $c_x^{su(3)_2}(q)$ denote the characters of the $su(3)_2$ parafermion theory. This theory has eight fields, including the identity field $\mathbf{1}$, with the character $c_{\mathbf{1}}^{su(3)_2}(q)$, and three parafermions, $\psi_1, \psi_2$, and $\psi_{12}$, which have identical characters $c_{\psi}^{su(3)_2}(q)$. The remaining four fields are three "spin" fields, $\sigma_1$, $\sigma_2$, and $\sigma_{12}$, which have identical characters $c_{\sigma}^{su(3)_2}(q)$. Finally, there is the field $\rho$, whose character we denote by $c_{\rho}^{su(3)_2}(q)$.

In the above, the characters of the fields are "normalized" such that the first term in the expansion is $q^h$, where $h$ is the conformal dimension of the field under consideration. These conformal dimensions are given by $h_{\mathbf{1}} = 0$, $h_{\psi} = \frac{1}{2}$, $h_{\sigma} = \frac{1}{10}$, and $h_{\rho} = \frac{3}{5}$. Combining all the factors, the expressions for the limit of $X_m(q)$ are series expansions with integer or half integer powers of $q$.

For our present proposes, it is best to view this CFT as the following coset model: $\frac{su(2)_1 \times su(2)_1 \times su(2)_1}{su(2)_3}$. The fields in this coset model are labeled by the labels of the constituent factors,

$\Phi_{l_4}^{l_1,l_2,l_3}$, where $l_1, l_2, l_3$ correspond to the factors su(2)$_1$, and $l_4$ corresponds to the factor su(2)$_3$. These labels have to satisfy the constraint $l_1 + l_2 + l_3 + l_4 = 0 \bmod 2$, which we use to set $l_1 = 0$, and consider the fields with $l_2 + l_3 + l_4 = 0 \bmod 2$.

For completeness, we explicitly give the labels of the parafermion fields:

$$\Phi_0^{0,0,0} = \mathbf{1}, \quad \Phi_0^{0,1,1} = \psi_1, \quad \Phi_3^{0,1,0} = \psi_2, \quad \Phi_3^{0,0,1} = \psi_{12},$$

$$\Phi_2^{0,0,0} = \rho, \quad \Phi_2^{0,1,1} = \sigma_2, \quad \Phi_1^{0,1,0} = \sigma_1, \quad \Phi_1^{0,0,1} = \sigma_{12}.$$

For $r > 5$, we did not yet obtain closed expressions for the functions $X_m(a; b, c, d, e; q)$. However, one can obtain expansions to high order, by making use of the recursion relations satisfied by the $X_m(q)$ [Eq. (D1)]. These high-order expansions can be compared to the branching functions (or characters) of various coset model. In doing so, we have established that the $X_m(a; b, c, d, e; q; r)$ are (in the limit $m \to \infty$) the characters of the cosets $\frac{\text{su}(2)_1 \times \text{su}(2)_1 \times \text{su}(2)_{k-2}}{\text{su}(2)_k}$ (we recall that $k = r - 2$). In Appendix D, we give the relation between the values $(a; b, c, d, e)$ and the labels of the coset fields.

### B. Probability amplitudes for $u < 0$

The functions $X_m(q)$, with the boundary heights $(b, c, d, e)$ given by the ground-state patterns for $u < 0$, can also be expressed in terms of the function $y(m; l_2, l_3, l_4)$, which was introduced in the previous section. We first state these results and subsequently take the limit $m \to \infty$ in order to identify the critical theory describing the critical behavior of the anyonic quantum spin chain. In particular, for $r = 5$,

$$X_m(1; 2, 1, 2, 1; q) = q^{\frac{m+1}{4}} y\left(\frac{m-1}{2}, 1, 1, 1\right),$$

$$X_m(1; 2, 3, 2, 3; q) = q^{\frac{m+1}{4}} y\left(\frac{m-1}{2}, 1, 2, 1\right),$$

$$X_m(1; 4, 3, 4, 3; q) = q^{\frac{m+1}{2}} y\left(\frac{m-1}{2}, 2, 2, 1\right),$$

$$X_m(2; 1, 2, 1, 2; q) = q^{\frac{m+1}{2}} y\left(\frac{m-1}{2}, 2, 2, 2\right), \quad (74)$$

$$X_m(2; 3, 2, 3, 2; q) = q^{\frac{m+1}{4}} y\left(\frac{m-1}{2}, 1, 2, 3\right),$$

$$X_m(2; 3, 4, 3, 4; q) = q^{\frac{m+1}{4}} y\left(\frac{m-1}{2}, 1, 1, 3\right).$$

The ground states correspond to the highest possible powers of $q$, so to make the identification with the CFT, we have to make the substitution $q \to q^{-1}$ and multiply by $q^{\frac{(m+1)(m+3)}{8}}$, which is the maximal power of $q$ which occurs in the functions $X_m(q)$. This will make sure that the function corresponding to the vacuum character is a polynomial in $q$, starting with 1. We find that the functions thus obtained tend to the characters of the su(2)$_3$ parafermions in the limit $m \to \infty$. The su(2)$_3$ parafermion theory contains six fields, the identity, with character $c_{\mathbf{1}}^{\text{su}(2)_3}$, two parafermion fields $\psi_1$ and $\psi_2$, with

the character $c_\psi^{\text{su}(2)_3}$, two spin fields $\sigma_1$ and $\sigma_2$, with characters $c_\sigma^{\text{su}(2)_3}$, and finally the field $\epsilon$, with the character $c_\epsilon^{\text{su}(2)_3}$. The scaling dimensions are $h_{\mathbf{1}} = 0$, $h_\psi = \frac{2}{3}$, $h_\sigma = \frac{1}{15}$, and $h_\epsilon = \frac{2}{5}$. We find

$$\lim_{p \to \infty} q^{\frac{(p+1)(p+2)}{2}} X_{2p+1}(1; 2, 1, 2, 1; q^{-1}) = c_{\mathbf{1}}^{\text{su}(2)_3}(q), \quad (75)$$

$$\lim_{p \to \infty} q^{\frac{(p+1)(p+2)}{2}} X_{2p+1}(1; 2, 3, 2, 3; q^{-1})$$

$$= \lim_{p \to \infty} q^{\frac{(p+1)(p+2)}{2}} X_{2p+1}(1; 4, 3, 4, 3; q^{-1}) = q^{-\frac{1}{6}} c_\psi^{\text{su}(2)_3}(q), \quad (76)$$

$$\lim_{p \to \infty} q^{\frac{(p+1)(p+2)}{2}} X_{2p+1}(2; 1, 2, 1, 2; q^{-1})$$

$$= \lim_{p \to \infty} q^{\frac{(p+1)(p+2)}{2}} X_{2p+1}(2; 3, 2, 3, 2; q^{-1}) = q^{-\frac{1}{15}} c_\sigma^{\text{su}(2)_3}(q), \quad (77)$$

$$\lim_{p \to \infty} q^{\frac{(p+1)(p+2)}{2}} X_{2p+1}(2; 3, 4, 3, 4; q^{-1}) = q^{\frac{1}{10}} c_\epsilon^{\text{su}(2)_3}(q). \quad (78)$$

The identification of the functions $X_m(q^{-1})$ for $u < 0$ in the limit $m \to \infty$ is given in Appendix D, in the case $k > 3$ ($r > 5$). They correspond to the characters of the $Z_k$ parafermions.[37]

### VIII. CONCLUSIONS AND OUTLOOK

We have introduced a 2D classical statistical mechanics model, the critical properties of which correspond to the integrable points of a chain of su(2)$_k$ anyons with competing two- and tree-body interactions [$J_2 - J_3$ model, given in Eq. (24)]. The 2D classical model is a composite height model which is a generalization of the RSOS model solved by ABF[8] by means of the CTM method. We have also used the CTM method and have found that, similar to the RSOS model, there are four different regimes with two critical points at $p = 0$. We have studied two new integrable critical points of the anyonic chain at $\tan \theta_{\text{int}} = (d_k^2 - 1)/d_k^2$, which correspond to the $p \to +0$, $u \to \pm 0$ limits of the composite height model.

For ferromagnetic interactions ($u > 0$, $\theta = \arctan[(d_k^2 - 1)/d_k^2] + \pi$, $J_2, J_3 < 0$) the critical point is described by the $\frac{\text{su}(2)_1 \times \text{su}(2)_1 \times \text{su}(2)_{k-2}}{\text{su}(2)_k}$ coset CFT. This critical behavior actually describes an extended critical region around the integrable point. For antiferromagnetic interactions ($u < 0$, $\theta = \arctan[(d_k^2 - 1)/d_k^2]$, $J_2, J_3 > 0$) the behavior is that of the $Z_k$ parafermions. This critical point constitutes the boundary between a gapped phase, and an extended critical region, which is described, in general, by the $\mathcal{M}(k + 1, k + 2)$ minimal model.[2]

These CFT identifications stem from the observations that functions $X_m(q)$, which define the local height probabilities are given by characters of the corresponding CFT. The integrable properties of quantum 1D and classical 2D models are fully defined by the Temperley-Lieb algebra relations in Eq. (9), which suggest that the Hamiltonian in Eq. (24) can be exactly solved in different representations of TL algebra. A particular physical interpretation of the model depends on the particular representation chosen to solve it. In our case,

we have used the representation of $su(2)_k$ anyons, which straightforwardly maps onto the composite RSOS model. In this representation, an interpretation as a chain of interacting anyons is straightforward.

A different interpretation as a $Q$-state Potts model [with $\sqrt{Q} = 2\cos(\frac{\pi}{k+2}) = d_k$, where in this case $k$ is considered to be a continuous parameter] or a six-vertex model was put forward by Ikhlef et al.,[17,18] which naturally admits the so called "loop representation." The $J_2 - J_3$ model at the integrable point, $\theta = \arctan[(d_k^2 - 1)/d_k^2] + \pi$, has been exactly solved in spin-$\frac{1}{2}$ representation of the $U_q[\mathrm{SU}(2)]$ quantum algebra.[17,18] In this representation, in contrast to the "anyon representation," the Hilbert space has a tensor product structure and the $J_2 - J_3$ model admits the solution by the algebraic Bethe ansatz method. We should note that in spin or loop representations the 1D quantum Hamiltonian is non-Hermitian and lacks obvious physical interpretation. Despite this non-Hermiticity, it has been conjectured that the part of the spectrum which scales as $1/L$ is real. In contrast, in the anyon representation, which is adopted in this paper, the Hamiltonian is Hermitian (real symmetric) and has a physical interpretation as a local interaction between anyons. Despite the differences, the critical properties at $\theta = \arctan[(d_k^2 - 1)/d_k^2] + \pi$ found by us are similar to those found by Ikhlef et al.[17,18] Namely, they have the same central charge, at least for $u$ positive. The precise connection between these models is interesting and requires more detailed research. We note that a similar loop model, related to the anyon model with $u < 0$ ($\theta = \arctan[(d_k^2 - 1)/d_k^2]$), has been studied in Ref. 38. It was conjectured and several arguments were given that the critical behavior of this loop model (in an appropriate limit) is described by $Z_k$ parafermions.

The anyonic chains have been generalized in different ways. the first is to different types of unitary anyons.[4] It would be very interesting to investigate to what extend the methods of "fused models," as studied in Refs. 12 and 31, can be applied to the anyonic chains of Ref. 4. Chains of nonunitary anyons were also considered.[39] This leads, in general, to non-Hermitian Hamiltonians, which nevertheless have a real spectrum. It should be possible to generalize the models considered in Ref. 40 to composite versions and make a connection with a generalization of the chains considered in Ref. 39.

In this paper, we have described only half of the phase diagram of the composite RSOS model, positive $p$ regime ($0 < p < 1$). The CTM method makes it possible to study the negative $p$ regime ($-1 < p < 0$) also, which will be addressed

in a subsequent publication. We have shown that the positive $p$ regime has the interpretation in terms of 1D interacting anyons. The 1D quantum mechanical interpretation of the negative $p$ regime is yet unknown and also requires further investigation.

Last, but not least, we would like to point out that the study of the RSOS model by ABF gave rise to an interesting set of Rogers-Ramanujan-type identities. Further study of the composite height model in light of these identities will be most interesting.

### APPENDIX A: THE PLAQUETTES OF THE COMPOSITE-RSOS MODEL

The plaquettes of the composite model are obtained by stacking four plaquettes of the original RSOS model (see Fig. 7), and giving them the appropriate weights. In the process of stacking the plaquettes, one has to sum over the internal height, which in some cases can take two possible values (see Fig. 8).

In the following, we display the possible composite plaquette types and give the associated weights in terms of the weights of the RSOS model. In this case, the composite plaquette weights have the same symmetry as the original model (with $\phi = 0$); namely, the weights are unchanged under exchange of the northwest (NW) and southeast (SE) corners, as well as under exchange of the northeast (NE) and southwest (SW) corners. This last property is lost if $\phi \neq 0, K$.

We start by giving the composite plaquettes for which the internal height is fixed by the boundary heights. In case the plaquette is not symmetric, we indicate the amount of plaquettes which can be obtained from the given by taking the appropriate mirror image. These mirrored plaquettes have the same weight as the displayed plaquette.

The weights of the composite plaquettes are given in terms of the weights of the original RSOS model, given in Eq. (18). Let $\zeta_l(u)$ be any weight of the RSOS model, that is, $\zeta = \alpha, \beta, \gamma, \delta$. Then, $\zeta_l = \zeta_l(u)$, $\zeta_l^+ = \zeta_l(u + K)$, and $\zeta_l^- = \zeta_l(u - K)$. With this notation, we can give the weights of the composite plaquettes for $\phi = K$:

$$
\begin{matrix} l & l+1 & l+2 \\ l-1 & & l+1 \\ l-2 & l-1 & l \end{matrix} = \beta_{l+1}^+ \beta_{l-1}^- \beta_l^2 \quad (\nearrow), \qquad
\begin{matrix} l+2 & l+1 & l \\ l+1 & & l-1 \\ l & l-1 & l-2 \end{matrix} = \alpha_l^+ \alpha_l^- \alpha_{l+1} \alpha_{l-1} \quad (\searrow), \tag{A1}
$$

$$
\begin{matrix} l-1 & l & l+1 \\ l-2 & & l \\ l-1 & l-2 & l-1 \end{matrix} = \beta_l^+ \gamma_{l-2}^- \beta_{l-1}^2 \quad (\nearrow), \qquad
\begin{matrix} l+1 & l & l-1 \\ l+2 & & l \\ l+1 & l+2 & l+1 \end{matrix} = \beta_l^+ \delta_{l+2}^- \beta_{l+1}^2 \quad (\nearrow), \tag{A2}
$$

$$\begin{matrix} l+1 & l & l-1 \\ l & & l-2 \\ l-1 & l-2 & l-1 \end{matrix} = \alpha_{l-1}^{+}\alpha_{l-1}^{-}\alpha_{l}\delta_{l-1} \quad (\searrow), \qquad \begin{matrix} l-1 & l & l+1 \\ l & & l+2 \\ l+1 & l+2 & l+1 \end{matrix} = \alpha_{l+1}^{+}\alpha_{l+1}^{-}\alpha_{l}\gamma_{l+1} \quad (\searrow), \qquad \text{(A3)}$$

$$\begin{matrix} l-1 & l & l+1 \\ l-2 & & l \\ l-1 & l & l-1 \end{matrix} = \beta_{l}^{+}\alpha_{l-1}^{-}\beta_{l-1}\gamma_{l-1} \quad (\boxtimes), \qquad \begin{matrix} l+1 & l & l-1 \\ l+2 & & l \\ l+1 & l & l+1 \end{matrix} = \beta_{l}^{+}\alpha_{l+1}^{-}\beta_{l+1}\delta_{l+1} \quad (\boxtimes), \qquad \text{(A4)}$$

$$\begin{matrix} l+1 & l & l-1 \\ l & & l \\ l-1 & l-2 & l-1 \end{matrix} = \delta_{l}^{+}\alpha_{l-1}^{-}\alpha_{l}\beta_{l-1} \quad (\boxtimes), \qquad \begin{matrix} l-1 & l & l+1 \\ l & & l \\ l+1 & l+2 & l+1 \end{matrix} = \gamma_{l}^{+}\alpha_{l+1}^{-}\alpha_{l}\beta_{l+1} \quad (\boxtimes), \qquad \text{(A5)}$$

$$\begin{matrix} l-1 & l & l+1 \\ l-2 & & l \\ l-1 & l & l+1 \end{matrix} = \beta_{l}^{+}\alpha_{l-1}^{-}\beta_{l-1}\alpha_{l} \quad (\boxtimes), \qquad \begin{matrix} l+1 & l & l-1 \\ l+2 & & l \\ l+1 & l & l-1 \end{matrix} = \beta_{l}^{+}\alpha_{l+1}^{-}\beta_{l+1}\alpha_{l} \quad (\boxtimes), \qquad \text{(A6)}$$

$$\begin{matrix} l & l+1 & l \\ l+1 & & l+1 \\ l & l-1 & l \end{matrix} = \delta_{l+1}^{+}\alpha_{l}^{-}\gamma_{l}\beta_{l} \quad (\boxtimes), \qquad \begin{matrix} l & l-1 & l \\ l-1 & & l-1 \\ l & l+1 & l \end{matrix} = \gamma_{l-1}^{+}\alpha_{l}^{-}\delta_{l}\beta_{l} \quad (\boxtimes), \qquad \text{(A7)}$$

$$\begin{matrix} l & l+1 & l \\ l-1 & & l+1 \\ l & l-1 & l \end{matrix} = \delta_{l+1}^{+}\gamma_{l-1}^{-}\beta_{l}^{2} \quad (\nearrow), \qquad \begin{matrix} l & l+1 & l \\ l-1 & & l-1 \\ l & l+1 & l \end{matrix} = \alpha_{l}^{+}\alpha_{l}^{-}\beta_{l}^{2} \quad (\searrow), \qquad \text{(A8)}$$

$$\begin{matrix} l & l+1 & l \\ l+1 & & l-1 \\ l & l-1 & l \end{matrix} = \alpha_{l}^{+}\alpha_{l}^{-}\gamma_{l}\delta_{l} \quad (\searrow). \qquad \text{(A9)}$$

We now focus on the composite plaquettes for which the internal height is not fixed by those of the boundary in general and hence takes two different values. The composite weight is a sum of two terms, the first term corresponding to the internal height being $l+1$ and the second one to the internal height $l-1$:

$$\begin{matrix} l+1 & l & l+1 \\ l & & l \\ l+1 & l & l+1 \end{matrix} = \gamma_{l}^{+}\gamma_{l}^{-}\delta_{l+1}^{2} + \beta_{l}^{+}\beta_{l}^{-}\alpha_{l}^{2}, \qquad \begin{matrix} l-1 & l & l-1 \\ l & & l \\ l-1 & l & l-1 \end{matrix} = \beta_{l}^{+}\beta_{l}^{-}\alpha_{l}^{2} + \delta_{l}^{+}\delta_{l}^{-}\gamma_{l-1}^{2}, \qquad \text{(A10)}$$

$$\begin{matrix} l+1 & l & l-1 \\ l & & l \\ l+1 & l & l+1 \end{matrix} = \beta_{l}^{+}\gamma_{l}^{-}\delta_{l+1}^{2} + \delta_{l}^{+}\beta_{l}^{-}\alpha_{l}^{2} \quad (\nearrow), \qquad \begin{matrix} l-1 & l & l+1 \\ l & & l \\ l-1 & l & l-1 \end{matrix} = \gamma_{l}^{+}\beta_{l}^{-}\alpha_{l}^{2} + \beta_{l}^{+}\delta_{l}^{-}\gamma_{l-1}^{2} \quad (\nearrow), \qquad \text{(A11)}$$

$$\begin{matrix} l-1 & l & l+1 \\ l & & l \\ l+1 & l & l+1 \end{matrix} = \gamma_{l}^{+}\gamma_{l}^{-}\delta_{l+1}\alpha_{l} + \beta_{l}^{+}\beta_{l}^{-}\alpha_{l}\gamma_{l-1} \quad (\searrow), \qquad \begin{matrix} l+1 & l & l-1 \\ l & & l \\ l-1 & l & l-1 \end{matrix} = \beta_{l}^{+}\beta_{l}^{-}\delta_{l+1}\alpha_{l} + \delta_{l}^{+}\delta_{l}^{-}\alpha_{l}\gamma_{l-1} \quad (\searrow),$$

$$\text{(A12)}$$

$$\begin{matrix} l+1 & l & l-1 \\ l & & l \\ l-1 & l & l+1 \end{matrix} = \beta_{l}^{+}\beta_{l}^{-}\delta_{l+1}^{2} + \delta_{l}^{+}\delta_{l}^{-}\alpha_{l}^{2}, \qquad \begin{matrix} l-1 & l & l+1 \\ l & & l \\ l+1 & l & l-1 \end{matrix} = \gamma_{l}^{+}\gamma_{l}^{-}\alpha_{l}^{2} + \beta_{l}^{+}\beta_{l}^{-}\gamma_{l-1}^{2}, \qquad \text{(A13)}$$

$$\begin{matrix} l-1 & l & l-1 \\ l & & l \\ l+1 & l & l+1 \end{matrix} = \beta_{l}^{+}\gamma_{l}^{-}\alpha_{l}\delta_{l+1} + \delta_{l}^{+}\beta_{l}^{-}\gamma_{l-1}\alpha_{l} \quad (\boxtimes). \qquad \text{(A14)}$$

We find that the total number of possible composite plaquette types is 66. The total number of plaquettes depends on the value of $r = k + 2$, as is the case in the RSOS model.

## APPENDIX B: PROPERTIES OF CORNER TRANSFER MATRICES IN DIFFERENT DOMAINS

To find out the properties of CTMs near the boundaries of different domains we need to calculate the weights of the composite model in those limits.

### 1. $u \to 0$ limit

Using the properties of the elliptic $\theta$ functions it is straightforward to show that the weights of the RSOS model in the $u \to 0$ limit are

$$\alpha_l(u=0) = 1, \quad \beta_l(u=0) = 0,$$
$$\gamma_l(u=0) = 1, \quad \delta_l(u=0) = 1. \tag{B1}$$

The RSOS wights with shifted fugacities, $\phi = K = \eta r$, have the form

$$\alpha_l^+(u=0) = -\alpha_l^-(u=0) = \frac{h(2\eta - \eta r)}{h(2\eta)},$$

$$\beta_l^+(u=0) = -\beta_l^-(u=0)$$
$$= \frac{h(\eta r)}{h(2\eta)} \frac{\{h[2\eta(l-1)]h[2\eta(l+1)]\}^{1/2}}{h(2\eta l)}, \tag{B2}$$

$$\gamma_l^+(u=0) = -\gamma_l^-(u=0) = \delta_l^-(u=0) = \frac{h(2\eta l + \eta r)}{h(2\eta l)},$$

$$\delta_l^+(u=0) = -\delta_l^-(u=0) = \gamma_l^-(u=0) = \frac{h(2\eta l - \eta r)}{h(2\eta l)}.$$

We are able to show that in this limit all off-diagonal (NE-SW asymmetric) weights of the composite model are zero and only diagonal (NE-SW symmetric) weights survive. This implies that the CTMs $A$ and $C$ are diagonal in this limit. Of the 66 different type of plaquettes, 50 are off-diagonal. Of these 50 type of plaquettes, 42 are trivially zero in the limit $u \to 0$, because they contain a factor $\beta_l(u=0) = 0$. The remaining plaquettes are those in Eqs. (A11) and (A14), and they are zero because of the relations between the weights given in Eq. (B2). As an example, we have for the plaquettes on left hand side of Eq. (A11): $\beta_l^+ \gamma_l^- \delta_{l+1}^2 + \delta_l^+ \beta_l^- \alpha_l^2 = \beta_l^+ \gamma_l^- + \delta_l^+ \beta_l^- = \beta_l^+ \delta_l^+ - \delta_l^+ \beta_l^+ = 0$.

The weights of all the diagonal plaquettes turn out to be the same. For the weights which only have one contributing term, we immediately find $W_1 = -(\frac{h(2\eta - \eta r)}{h(2\eta)})^2$. The weights of the diagonal plaquettes which consist of two terms read $W_2 = -(\frac{h(2\eta l - \eta r)}{h(2\eta l)})^2 - (\frac{h(\eta r)}{h(2\eta)h(2\eta l)})^2 h(2\eta l - 2\eta)h(2\eta l + 2\eta)$. By making use of the following identity for elliptic functions (see, for instance, Chapter 15 of Ref. 9),

$$h^2(2\eta - \eta r)h^2(2\eta l) = h^2(2\eta)h^2(2\eta l - \eta r)$$
$$+ h^2(\eta r)h[2\eta(l-1)]h[2\eta(l+1)], \tag{B3}$$

we find that $W_2 = W_1$. Thus, the general weight of the composite model reads, in the limit $u \to 0$,

$$\tilde{W}(l_1, l_2, l_3, l_4, l_5, l_6, l_7, l_8)(u=0)$$
$$= -\left(\frac{h(2\eta - \eta r)}{h(2\eta)}\right)^2 \delta_{l_2, l_8} \delta_{l_3, l_7} \delta_{l_4, l_6}. \tag{B4}$$

Using the definition of $U_j$ [Eq. (40)], we can show that

$$(U_j)_{\mathbf{l},\mathbf{l}'}(u=0) = -\left(\frac{h(2\eta - \eta r)}{h(2\eta)}\right)^2 \delta(\mathbf{l}, \mathbf{l}'), \tag{B5}$$

such that $U_j$ is a diagonal matrix. From the above and Eq. (42) it follows that

$$A(u=0) = C(u=0) = \mathbb{1}, \tag{B6}$$

where we have dropped the irrelevant multiplicative factor, which only depends on $r$.

### 2. $u \to (2+r)\eta$ limit

We show that in the limit $u \to (2+r)\eta$, the CTMs $B$ and $D$ are diagonal. For unshifted weights of the RSOS model in the $u \to (2+r)\eta$ limit we get

$$\alpha_l[u = (2+r)\eta] = -\frac{h(\eta r)}{h(2\eta)},$$

$$\beta_l[u = (2+r)\eta] = -\frac{h(2\eta - \eta r)}{h(2\eta)} \frac{\{h[2\eta(l-1)]h[2\eta(l+1)]\}^{1/2}}{h(2\eta l)},$$

$$\gamma_l[u = (2+r)\eta] = -\frac{h[2\eta(l+1) - \eta r]}{h(2\eta l)},$$

$$\delta_l[u = (2+r)\eta] = \frac{h[2\eta(l-1) - \eta r]}{h(2\eta l)}. \tag{B7}$$

The shifted weights take the form

$$\alpha_l^+[u = (2+r)\eta] = \alpha_l^-[u = (2+r)\eta] = 0,$$
$$\beta_l^+[u = (2+r)\eta] = -\beta_l^-[u = (2+r)\eta]$$
$$= -\frac{\{h[2\eta(l-1)]h[2\eta(l+1)]\}^{1/2}}{h(2\eta l)},$$

$$\gamma_l^+[u = (2+r)\eta] = -\gamma_l^-[u = (2+r)\eta] = -\frac{h[2\eta(l+1)]}{h(2\eta l)},$$

$$\delta_l^+[u = (2+r)\eta] = -\delta_l^-[u = (2+r)\eta] = -\frac{h[2\eta(l-1)]}{h(2\eta l)}. \tag{B8}$$

Because $\alpha_l^+[u = (2+r)\eta] = \alpha_l^-[u = (2+r)\eta] = 0$, most of the NW-SE asymmetric weights are zero. The remaining NW-SE asymmetric weights can be shown to be zero, by making use of the properties Eqs. (B7) and (B8). This shows that for $u \to (2+r)\eta$, the CTMs $B$ and $D$ are diagonal.

As was the case for $u=0$, the plaquettes which contribute in the limit $u \to (2+r)\eta$ fall into two classes, the ones with one term and those with two terms. Again, the plaquette weights of these two classes can be shown to give rise to the same weights, by making use of the elliptic function relation in Eq. (B3). The final form of the weights is slightly more complicated than in the case $u=0$ and does, in fact, depend on the heights,

$$\tilde{W}(l_1, l_2, l_3, l_4, l_5, l_6, l_7, l_8)[u = (2+r)\eta]$$
$$= -\frac{[h(2\eta l_3)h(2\eta l_7)]^{1/2}}{h(2\eta l_1)} \left(\frac{h(2\eta - \eta r)}{h(2\eta)}\right)^2 \delta_{l_1, l_5} \delta_{l_2, l_4} \delta_{l_6, l_8}. \tag{B9}$$

Using the definition of $V_j$ [Eq. (41)], we can show that

$$V_j[u = (2+r)\eta] = -\left(\frac{h(2\eta - \eta r)}{h(2\eta)}\right)^2 \tilde{V}_{2j-1}\tilde{V}_{2j+3}\tilde{V}^{-2}_{2j+1},$$

$$(\text{B10})$$

where we introduced

$$(\tilde{V}_j)_{\mathbf{l},\mathbf{l}'} = [h(2\eta l_j)]^{1/2}\delta(\mathbf{l},\mathbf{l}').\qquad(\text{B11})$$

From the above and the definition of the CTMs [Eq. (42)], it follows that

$$B[u = (2+r)\eta] = D[u = (2+r)\eta] = \tilde{V}_1,\quad(\text{B12})$$

where we again dropped the irrelevant ($l_1$ independent) multiplicative factor.

### 3. $u \to (2-r)\eta$ limit

In this limit all the weights of the RSOS model just change sign compared to the $u \to (2+r)\eta$ limit. Hence, the weights of the composite model are unchanged and we find

$$B[u = (2-r)\eta] = D[u = (2-r)\eta] = \tilde{V}_1.\quad(\text{B13})$$

## APPENDIX C: WEIGHTS OF THE COMPOSITE MODEL IN THE $p \to 1$ LIMIT

To derive the integer function $N(\mathbf{l})$, we consider the limit $p \to 1$, where weights of the composite model, and hence the CTM $A$, become diagonal. For $0 < p < 1$, employing the conjugate modulus transformation, the function $h(u)$ can be written in the following way[8]:

$$h(u) = \tau \exp\left[-\frac{\pi(u-K)^2}{2KK'}\right]E(e^{-2\pi u/K'}, y),\quad(\text{C1})$$

where

$$y = e^{-4\pi K/K'},\quad \tau = \frac{K}{K'}\prod_{n=1}^{\infty}\frac{1 - y^{n/2}}{1 + y^{n/2}},\quad(\text{C2})$$

and the function $E(z,x)$ is Jacobi's triple product

$$E(z,x) = \prod_{n=1}^{\infty}(1 - x^{n-1}z)(1 - x^n z^{-1})(1 - x^n).\quad(\text{C3})$$

Then the weights of the RSOS model have the form

$$\alpha_l = v\frac{g_l^2}{g_{l-1}g_{l+1}}w^{1/2}\frac{E(xw^{-1}, x^r)}{E(x, x^r)},$$

$$\beta_l = v\frac{g_{l-1}g_{l+1}}{g_l^2}\left(\frac{xE(x^{l-1}, x^r)E(x^{l+1}, x^r)}{wE^2(x^l, x^r)}\right)^{1/2}\frac{E(w, x^r)}{E(x, x^r)},$$

$$\gamma_l = v\left(\frac{g_{l+1}}{g_l}\right)^2\frac{E(x^l w, x^r)}{E(x^l, x^r)},$$

$$\delta_l = v\left(\frac{g_{l-1}}{g_l}\right)^2\frac{E(x^l w^{-1}, x^r)}{E(x^l, x^r)},\quad(\text{C4})$$

where

$$x = e^{-4\pi\eta/K'},\quad w = e^{-2\pi u/K'},$$

$$g_l = \exp\left[-\frac{\pi u(2\eta l - K)^2}{8\eta KK'}\right],\quad(\text{C5})$$

and $v$ is a constant independent of $l$.

In what follows, we show that in the limit of $p \to 1$ and $w \to 1$ the weights of the composite model become diagonal (similar to the RSOS model). It is straightforward to see that the limit $p \to 1$ implies that $x \to 0$, since $K'(p \to 1)$ diverges. To find out the limiting values of the weights, we use the following properties of the function $E(z,x)$:

$$\lim_{x\to 0} E(x^l w, x^r) = \begin{cases} 1 - w & l = 0, \\ 1 & 1 \leqslant l \leqslant r - 1, \end{cases}\quad(\text{C6})$$

$$\lim_{x\to 0} E(wx^{l+r/2}, x^r) = \begin{cases} 1 & 0 \leqslant l < r/2, \\ 1 - w^{-1} & l = r/2, \\ -wx^{r/2-l} & r/2 < l \leqslant r - 1, \end{cases}\quad(\text{C7})$$

$$\lim_{x\to 0} E(wx^{l-r/2}, x^r) = \begin{cases} -wx^{l-r/2} & 0 \leqslant l < r/2, \\ 1 - w & l = r/2, \\ 1 & r/2 < l \leqslant r - 1. \end{cases}\quad(\text{C8})$$

In this limit the weights of the RSOS model (unshifted as well as shifted) can be written as

$$
\begin{aligned}
&\alpha_l = w^{\frac{r-1}{2r}}, &&\alpha_l^+ = -w^{-\frac{r+1}{2r}}x^{\frac{3-r}{4}}, &&\alpha_l^- = w^{\frac{r-1}{2r}}x^{\frac{1-r}{4}},\\
&\beta_l = (1-w)w^{-\frac{r-1}{2r}}x^{\frac{1}{2}}, &&\beta_l^+ = w^{\frac{1-r}{2r}}x^{\frac{3-r}{4}}, &&\beta_l^- = -w^{\frac{1+r}{2r}}x^{\frac{1-r}{4}},\\
&\gamma_l = w^{\frac{1+2l-r}{2r}}, &&\gamma_l^+ = \begin{cases} w^{\frac{1+2l-r}{2r}}x^{\frac{1+2l-r}{4}} & l < \frac{r}{2},\\ w^{\frac{1}{2r}}(1 - \frac{1}{w})x^{\frac{1}{4}} & l = \frac{r}{2},\\ -w^{\frac{1+2l-3r}{2r}}x^{\frac{1-2l+r}{4}} & l > \frac{r}{2}, \end{cases} &&\gamma_l^- = \begin{cases} -w^{\frac{1+2l-r}{2r}}x^{\frac{-1+2l-r}{4}} & l < \frac{r}{2},\\ w^{\frac{1}{2r}}(1-w)x^{-\frac{1}{4}} & l = \frac{r}{2},\\ w^{\frac{1+2l-r}{2r}}x^{\frac{-1-2l+r}{4}} & l > \frac{r}{2}, \end{cases}\\
&\delta_l = w^{\frac{1-2l+r}{2r}}, &&\delta_l^+ = \begin{cases} -w^{\frac{1-2l-r}{2r}}x^{\frac{1+2l-r}{4}} & l < \frac{r}{2},\\ w^{\frac{1}{2r}}(1 - \frac{1}{w})x^{\frac{1}{4}} & l = \frac{r}{2},\\ w^{\frac{1-2l+r}{2r}}x^{\frac{1-2l+r}{4}} & l > \frac{r}{2}, \end{cases} &&\delta_l^- = \begin{cases} w^{\frac{1-2l+r}{2r}}x^{\frac{-1+2l-r}{4}} & l < \frac{r}{2},\\ w^{\frac{1}{2r}}(1-w)x^{-\frac{1}{4}} & l = \frac{r}{2},\\ -w^{\frac{1-2l+3r}{2r}}x^{\frac{-1-2l+r}{4}} & l > \frac{r}{2}. \end{cases}
\end{aligned}
\quad(\text{C9})
$$

Using the limits above and taking into account the exact forms for the composite weights (see Appendix A), we are able to show that the diagonal weights become much larger than the off-diagonal ones. In particular, the leading $x$ behavior of the weights of the diagonal plaquettes (those which are NE-SW symmetric) is given by $x^{1-r/2}$, in the limit $x \to 0$. We explicitly checked that all the off-diagonal plaquettes have weights with a leading exponent of $x$ strictly larger than $1 - r/2$, showing that $A$ is diagonal when $p \to 1$. So in this limit we can drop all the off-diagonal weights and only diagonal weights contribute to the CTM:

$$\tilde{W}(l_1, l_2, l_3, l_4, l_5, l_6, l_7, l_8)$$
$$= \frac{g_{l_3} g_{l_7}}{g_{l_1} g_{l_5}} x^{1-r/2} w^{|l_1 - l_5|/4 + \delta_{l_1,l_7} \delta_{l_6,l_8} \delta_{l_1,l_5}} \delta_{l_2,l_8} \delta_{l_3,l_7} \delta_{l_4,l_6}. \quad \text{(C10)}$$

The dependence on $w$ of the weights in the limit $p \to 1$ follows from the form of the weights $\alpha_l$, etc., given in Eq. (C9), combined with the form of the weights given in Eq. (C4). Note that the exponent of $w$ is always integer or half integer.

Inserting the above in the definition $A$ in Eq. (42), we get that

$$A_{\mathbf{l},\mathbf{l}'} = \prod_{j=1}^{(m+1)/2} [\tilde{W}(l_{2j-1}, l_{2j}, l_{2j+1}, l_{2j+2}, l_{2j}, l_{2j+1},$$
$$l_{2j+2}, l_{2j+3})]^j \delta(\mathbf{l}, \mathbf{l}') \quad \text{(C11)}$$

and

$$A_{\mathbf{l},\mathbf{l}'} = g_{l_1}^{-1} w^{\phi(\mathbf{l})} \delta(\mathbf{l}, \mathbf{l}'), \quad \text{(C12)}$$

where we have dropped the irrelevant multiplicative factor $x^{1-r/2}$ and $\phi(\mathbf{l})$ is given in Eq. (60).

## APPENDIX D: CONNECTION WITH CONFORMAL FIELD THEORY FOR $r > 5$

In the case $r > 5$, we did not yet obtain explicit expressions for the functions $X_m(q)$ with $m$ finite. However, the functions $X_m(q)$, with $m$ odd, satisfy the following recursion relations ($m$ is odd by definition):

$$X_m(a; b, c, d, e; q) = q^{\frac{(m+1)(|b-1-e|/4+\delta_{b-1,c}\delta_{c,e}\delta_{b,d})}{2}} X_{m-2}(a; b-2, b-1, b, c; q) + q^{\frac{(m+1)(|b-1-e|/4+\delta_{b-1,c}\delta_{c,e}\delta_{b,d})}{2}} X_{m-2}(a; b, b-1, b, c; q)$$
$$+ q^{\frac{(m+1)(|b+1-e|/4+\delta_{b+1,c}\delta_{c,e}\delta_{b,d})}{2}} X_{m-2}(a; b, b+1, b, c; q) + q^{\frac{(m+1)(|b+1-e|/4+\delta_{b+1,c}\delta_{c,e}\delta_{b,d})}{2}} X_{m-2}(a; b+2, b+1, b, c; q), \quad \text{(D1)}$$

where we define $X_m(a; b, c, d, e; q)$ to be zero if any of the $a, b, c, d, e$ lies outside of the range $1, 2, \ldots, r - 1$. In addition, $X_m(a; b, c, d, e; q) = 0$ if $|b - c| \neq 1$, $|c - d| \neq 1$, $|d - e| \neq 1$. Finally, $X_1(a; b, c, d, e; q) = q^{|a-e|/4 + \delta_{a,c}\delta_{b,d}\delta_{c,e}}$, if also $|a - b| = 1$ and zero otherwise.

Using these recursion relations, one can obtain high-order expansions for $X_m(q)$, which allows one to identify the CFT, by direct comparison to the CFT characters. The following exact results were obtained in this way and hence not proven.

### 1. The case $u > 0$ (domain $\mathcal{D}_1$)

For $u > 0$, we could identify the functions $X_m(q)$, where $(a; b, c, d, e)$ correspond to ground-state patterns, as characters of the coset model $\frac{su(2)_1 \times su(2)_1 \times su(2)_{k-2}}{su(2)_k}$, where $r - 2 = k \geqslant 3$. The ground states for $u > 0$ are discussed in Sec. VI A. The fields in this model are labeled by $\Phi_{s_2}^{t',t,s_1}$, where $t'$ and $t$ correspond to the factors $su(2)_1$, $s_1$ corresponds to $su(2)_{k-2}$, and $s_2$ to $su(2)_k$. Because of the constraint $t' + t + s_1 + s_2 = 0 \mod 2$, we can set $t' = 1$ (both $t'$ and $t$ can take the values 1

and 2). Finally, $s_1 = 1, 2, \ldots, k - 1$ and $s_2 = 1, 2, \ldots, k + 1$. Note that we use the height values to label the fields.

To make the connection between the labels $(t', t, s_1, s_2)$, we assume that $m = 4p + 3$, with $p$ an integer (the case $m = 4p + 1$ is very similar). Because of the relation $X_m(a; b, c, d, e; q) = X_m(r - a; r - b, r - c, r - d, r - e; q)$, we only have to consider two cases for the labels $(a; b, c, d, e)$. The function $\lim_{p \to \infty} X_{4p+3}(a; b, b - 1, b, b + 1; q)$ gives the character of the field $\Phi_a^{1,1,b-1}$. Finally, the function $\lim_{p \to \infty} X_{4p+3}(a; b, b+1, b+2, b+1; q)$ gives character of the fields $\Phi_a^{1,2,b}$.

For completeness, we give the scaling dimensions of the fields in the coset theory explicitly. This formula resembles the formula for the scaling dimensions of the minimal models.[41]

Finding the scaling dimensions of the fields in coset conformal field theories is typically easiest done in a Coulomb gas formalism.[42] In the case at hand, the relevant Coulomb gas was studied in Ref. 18. Based on those results we find (by appropriately constraining the values of the electric and magnetic charges)

$$h(t, s_1, s_2) = \begin{cases} \frac{[s_1(k+2) - s_2 k]^2 - 4}{8k(k+2)} + \frac{1}{2} - \frac{(s_1 - s_2 + 2t) \bmod 4}{4} & \text{for} \quad s_1 + s_2 \bmod 2 = 0, \\ \frac{[s_1(k+2) - s_2 k]^2 - 4}{8k(k+2)} + \frac{1}{8} & \text{for} \quad s_1 + s_2 \bmod 2 = 1. \end{cases} \quad \text{(D2)}$$

The scaling dimensions satisfy $h(3 - t, k - s_1, k + 2 - s_2) = h(t, s_1, s_2)$, reflexing the fact that the fields $\Phi_{k+2-s_2}^{3-t',3-t,k-s_1}$ and $\Phi_{s_2}^{t',t,s_1}$ are identified.

### 2. The case $u < 0$ (domain $\mathcal{D}_2$)

For $u < 0$, the system is described in terms of $Z_k$ parafermions, and we find the following identification. The $Z_k$ parafermion fields are labeled by two integers, $\Phi_n^j$, where $j = 0, 1, \ldots, k$, and $j + n = 0 \bmod 2$. Two fields which only differ in their $n$ label by $2k$ are identified, $\Phi_n^j \equiv \Phi_{n+2k}^j$. In addition, one has the identification $\Phi_n^j \equiv \Phi_{n+k}^{k-j}$, which is reflected in the function $X_m(q)$ via $X_m(a; b, c, d, e; q) = X_m(r - a; r - b, r - c, r - d, r - e; q)$. We remind the reader that $k = r - 2$ and that the parameters $a, \ldots, e$ lie in the range $1, 2, \ldots r - 1$.

For $u < 0$, the ground states are specified uniquely by $(a; b, c)$, because $d = b$ and $e = c$ (the ground states for $u < 0$ were discussed in Sec. VI B). Note that $c = b \pm 1$. The label $a$ corresponds directly to the label $j = a - 1$. The magnitude of the field label $n$ is given by $c - 1$, with a positive sign if $c = b + 1$ and a negative sign if $c = b - 1$. Thus, in general, we find that $\lim_{m \to \infty} q^{(m+1)(m+3)/8} X_m(a; b, c, b, c; q^{-1})$ corresponds to the character of the field $\Phi_{(c-b)(c-1)}^{a-1}$, where the limit is taken over the odd integers.

*Current address: Center for Materials Theory, Rutgers University, Piscataway, New Jersey 08854, USA.

[1]G. Moore and N. Read, Nucl. Phys. B **360**, 362 (1991).

[2]A. Feiguin, S. Trebst, A. W. W. Ludwig, M. Troyer, A. Kitaev, Z. Wang, and M. H. Freedman, Phys. Rev. Lett. **98**, 160409 (2007).

[3]S. Trebst, E. Ardonne, A. Feiguin, D. A. Huse, A. W. W. Ludwig, and M. Troyer, Phys. Rev. Lett. **101**, 050401 (2008).

[4]C. Gils, E. Ardonne, S. Trebst, A. W. W. Ludwig, M. Troyer, and Z. Wang, Phys. Rev. Lett. **103**, 070401 (2009).

[5]A. W. W. Ludwig, D. Poilblanc, S. Trebst, and M. Troyer, New J. Phys. **13**, 045014 (2011).

[6]E. Grosfeld and K. Schoutens, Phys. Rev. Lett. **103**, 076803 (2009).

[7]F. A. Bais, J. K. Slingerland, and S. M. Haaker, Phys. Rev. Lett. **102**, 220403 (2009).

[8]G. E. Andrews, R. J. Baxter, and P. J. Forrester, J. Stat. Phys. **35**, 193 (1984).

[9]R. J. Baxter, *Exactly Solved Models in Statistical Mechanics* (Academic Press, London, 1982).

[10]D. A. Huse, Phys. Rev. B **30**, 3908 (1984).

[11]H. Saleur and M. Bauer, Nucl. Phys. B **320**, 591 (1989).

[12]E. Date, M. Jimbo, A. Kuniba, T. Miwa, and M. Okado, Nucl. Phys. B **290**, 231 (1987).

[13]R. Kedem, R. R. Klassen, B. M. McCoy, and E. Melzer, Phys. Lett. B **307**, 68 (1993).

[14]F. D. M. Haldane, Phys. Rev. Lett. **67**, 937 (1991).

[15]K. Schoutens, Phys. Rev. Lett. **79**, 2608 (1997).

[16]S. Guruswamy and K. Schoutens, Nucl. Phys. B **556**, 530 (1999).

[17]Y. Ikhlef, J. L. Jacobsen, and H. Saleur, J. Phys. A **42**, 292002 (2009).

[18]Y. Ikhlef, J. L. Jacobsen, and H. Saleur, J. Phys. A **43**, 225201 (2010).

[19]C. Gils, E. Ardonne, S. Trebst, D. A. Huse, A. W. W. Ludwig, M. Troyer, and Z. Wang (unpublished).

[20]S. Trebst, M. Troyer, Z. Wang, and A. W. W. Ludwig, Prog. Theor. Phys. Suppl. **176**, 384 (2008).

[21]A. N. Kirillov and N. Y. Reshetikhin, in *Infinite Dimensional Lie Algebras and Groups, Proceedings of the Conference Held at CIRM, Luminy, Marseille*, edited by V. G. Kac (World Scientific, Singapore, 1988), p. 285.

[22]C. K. Majumdar and D. K. Ghosh, J. Math. Phys. **10**, 1388 (1969).

[23]C. K. Majumdar and D. K. Ghosh, J. Math. Phys. **10**, 1399 (1969).

[24]S. Trebst, D. A. Huse, E. Ardonne, A. Feiguin, A. W. W. Ludwig, and M. Troyer (upublished).

[25]D. Gepner, Nucl. Phys. B **290**, 10 (1987).

[26]A. B. Zamolodchikov and V. A. Fateev V. A, Zh. Eksp. Teor. Fiz. **89**, 380 (1985).

[27]V. Pasquier, Nucl. Phys. B **285**, 162 (1987).

[28]The parameter $u$ is related to $v$ in Ref. 8 by $u = \eta - v$.

[29]V. E. Korepin, N. M. Bogoliubov, and A. G. Izergin, *Quantum Inverse Scattering Method and Correlation Functions* (Cambridge University Press, Cambridge, 1993).

[30]This way of constructing a composite $R$ matrix is similar to the techniques for constructing higher spin, or "fused," models (see Refs. 12 and 13).

[31]W. M. Koo and H. Saleur, Int. J. Mod. Phys. A **8**, 5165 (1993).

[32]V. F. R. Jones, Invent. Math. **72**, 1 (1983).

[33]H. Wenzl, C. R. Math. Rep. Acad. Sci. Can. **9**, 5 (1987).

[34]R. J. Baxter, J. Phys. A **40**, 12577 (2007).

[35]E. Ardonne, N. Read, E. Rezayi, and K. Schoutens, Nucl. Phys. B **607**, 549 (2001).

[36]E. Ardonne and K. Schoutens, Phys. Rev. Lett. **82**, 5096 (1999).

[37]G. Georgiev, *Combinatorial Constructions of Modules for Infinite-dimensional Lie Algebras. II. Parafermionic Space*, e-print arXiv:q-alg/9504024.

[38]J. L. Jacobsen, H. Saleur, Nucl. Phys. B **743**, 207 (2006).

[39]E. Ardonne, J. Gukelberger, A. W. W. Ludwig, S. Trebst, and M. Troyer, New J. Phys. **13**, 045006 (2011).

[40]P. J. Forrester and R. J. Baxter, J. Stat. Phys. **38**, 435 (1985).

[41]A. A. Belavin, A. M. Polyakov, and A. B. Zamolodchikov, Nucl. Phys. B **241**, 333 (1984).

[42]Vl.S. Dotsenko and V. A. Fateev, Nucl. Phys. B **240**, 312 (1984).